Politecnico di Torino

Porto Institutional Repository

[Article] C0 triangular elements based on the Refined Zigzag Theory for multilayered composite and sandwich plates

(Article begins on next page)

C⁰ TRIANGULAR ELEMENTS BASED ON THE REFINED ZIGZAG THEORY FOR MULTILAYER COMPOSITE AND SANDWICH PLATES

Daniele Versino [a,], Marco Gherlone [a], Massimiliano Mattone [a], Marco Di Sciuva [a] and Alexander Tessler [b]*

[a] *Department of Mechanical and Aerospace Engineering*
Politecnico di Torino
Corso Duca degli Abruzzi 24, 10129, Torino, Italy

[b] *Structural Mechanics and Concepts Branch*
NASA Langley Research Center
Mail Stop 190, Hampton, Virginia, 23681 - 2199, U.S.A.

[*] *Corresponding author. Tel.: +39 011 0906807; fax: +39 011 0906899.*
E-mail address: daniele.versino@polito.it

ABSTRACT

The Refined Zigzag Theory (RZT) has been recently developed for the analysis of homogeneous, multilayer composite and sandwich plates. The theory has a number of practical and theoretical advantages over the widely used First-order Shear Deformation Theory (FSDT) and other types of higher-order and zigzag theories. Using FSDT as a baseline, RZT takes into account the stretching, bending, and transverse shear deformations. Unlike FSDT, this novel theory does not require shear correction factors to yield accurate results for a wide range of material systems including homogeneous, laminated composite, and sandwich laminates. The inplane zigzag kinematic assumptions, which compared to FSDT add two additional rotation-type kinematic variables, give rise to two types of transverse shear strain measures – the classical average shear strain (as in FSDT) and another one related to the cross-sectional distortions enabled by the zigzag kinematic terms. Consequently, with a fixed number of kinematic variables, the theory enables a highly accurate modeling of multilayer composite and sandwich plates even when the laminate stacking sequence exhibits a high degree of transverse heterogeneity. Unlike most zigzag formulations, this theory is not affected by such theoretical anomalies as the vanishing of transverse shear stresses and forces along clamped boundaries.

In this paper, six- and three-node, C^0-continuous, RZT-based triangular plate finite elements are developed; they provide the best compromise between computational efficiency and accuracy. The element shape functions are based on anisoparametric (aka interdependent) interpolations that ensure proper element behavior even when very thin plates are modeled. Continuous edge constraints are imposed on the transverse shear strain measures to derive coupled-field deflection shape functions, resulting in a simple and efficient three-node element. The elements are implemented in ABAQUS – a widely used commercial finite element code – by way of a user-element subroutine.

The predictive capabilities of the new elements are assessed on several elasto-static problems, which include simply supported and cantilevered laminated composite and sandwich plates. The numerical results demonstrate that the new RZT-based elements provide superior predictions for modeling a wide range of laminates including highly heterogeneous sandwich laminations. They also offer substantial improvements over the existing plate elements based on FSDT as well as other higher-order and zigzag-type elements.

KEYWORDS

Refined Zigzag Theory; First-order Shear Deformation Theory; Variational principle; Plate finite element; Shear locking; Transverse shear stresses; Composite plate; Sandwich plate.

1. INTRODUCTION

Laminated composite and sandwich plates and shells are widely used for military and civilian aircraft, aerospace vehicles, and naval and civil structures because of their high specific stiffness and strength and tailoring capabilities. Composite materials are increasingly adopted for primary load-bearing structures in the form of thick laminates with a large number of layers. Such laminated composite structures are inherently heterogeneous and anisotropic; they may exhibit design- and failure-critical deformation effects due to transverse shearing and transverse-normal stretching, with the consequential susceptibility to environmental and interlaminar-damage effects. Thus, accurate and computationally efficient models capable of incorporating these second-order effects are required for the design and analysis of multilayer composites.

Two main modeling strategies for composite structures can be found in the open literature: (i) models that only have displacements as the primary unknowns [1] and (ii) mixed models with displacements and stresses (commonly, transverse stresses) as unknowns [2]. Moreover, depending on the assumed distribution along the thickness for the primary unknowns, there may be [3]: (a) Equivalent Single Layer (ESL) theories, in which through-the-thickness distributions of the unknowns are assumed a priori over the total laminate thickness, and (b) Layer-Wise (LW) theories, in which the distribution of the unknowns is assumed layer by layer.

Among the ESL models that are based on displacements, classical lamination theories are often referred to: the Classical Lamination Plate Theory (CLPT) [4] and the First-order Shear Deformation Theory (FSDT) [5,6]. Their main merits are ease of implementation and adequate accuracy in terms of global response quantities such as displacements, natural frequencies, and buckling loads. These theories perform well for thin and moderately thick laminates that have a relatively low degree of transverse heterogeneity; however, their accuracy diminishes rapidly when highly heterogeneous and/or thick composite and sandwich laminates are modeled [1,7-9]. Improved predictions can be obtained using higher order through-the-thickness distributions of the displacements and/or stresses [10]. Computationally efficient analytical models for beams, plates and shells that account for transverse shear and thickness-stretch deformations have recently been advanced in [11-13]. The LW models [14-17] are generally very accurate but computationally costly; in these models the number of unknowns increases with the number of layers. This is especially relevant for nonlinear and/or progressive failure analyses of thick laminates made up of hundreds of layers, where the LW modeling is prohibitively expensive.

A meaningful compromise between acceptable accuracy and low computational cost is offered by the so-called zigzag theories [18-31]. In these theories (as in ESL), the number of kinematic unknowns does not depend on the number of layers; the LW-based zigzag theories have also been explored in [17]. The in-plane displacements combine the polynomial functions defined across the entire laminate thickness (linear [18-25] or cubic [26-31]) with the piecewise linear (i.e., *zigzag*) distributions. The zigzag contributions enable a more realistic modeling of the inplane cross-sectional distortion in multilayer composites, giving rise to a computationally efficient theory for the modeling of relatively thick laminated composite and sandwich structures. The zigzag-

theory predictions are often as accurate as those obtained by the computationally expensive LW and higher-order theories.

Averill [25] pointed out that there remain at least two key impediments for the analytical and computational applications of the zigzag theories. The key issues are that: (1) the transverse shear stresses derived from the constitutive equations vanish erroneously along clamped boundaries, and that (2) C^1-continuous finite element approximations are required for the transverse deflection variable − the type of approximation that is particularly undesirable for plate and shell elements.

To resolve the aforementioned issues, Tessler et. al. developed the Refined Zigzag Theory (RZT) [32-39] that makes use of a set of novel zigzag functions and uses FSDT as a baseline. The transverse shear stresses are allowed to be discontinuous along the ply interfaces; this relaxation of stress continuity permits more accurate predictions of all response quantities including the transverse shear stresses that provide accurate average values of the ply-level stresses. The key drawbacks of the original zigzag theories are overcome: (1) transverse shear stresses and forces do not vanish erroneously along clamped edges, and (2) since the strains are defined in term of first derivatives of the kinematic variables, computationally efficient C^0-continuous elements are readily formulated. The RZT has shown to be very accurate over a wide range of aspect ratios and material systems, including thick laminates with a high degree of transverse shear flexibility and heterogeneity [32-39].

Although computationally desirable and extensively used in commercial finite-element codes, C^0-continuous bending elements need to be designed to pass the *shear locking* barrier. When exact integration is used to compute the transverse shear strain energy, FSDT plate elements formulated with linear isoparametric shape functions produce overly stiff solutions when modeling thin plates. The reduced integration of the transverse shear energy alleviates shear locking; however, when applied to plate elements [40], reduced integration elements commonly give rise to non-physical zero-energy modes that must be eliminated with ad-hoc techniques. The use of higher-order polynomial shape functions generally improves thin-regime predictions. Several other successful approaches have been proposed to alleviate shear locking: penalty constraints, penalty-relaxation parameters, rotational bubble modes, and *anisoparametric* interpolations (the terms *interdependent* and *linked* interpolations have also been used [41,42].) The anisoparametric interpolation strategy, advanced by Tessler and co-workers for beam, plate, and shell elements [43-58], requires that the

transverse displacement is approximated with a complete polynomial one degree higher than the bending rotations (*unconstrained anisoparametric* element). Moreover, elements with isoparametric-like topologies can be readily obtained by condensing out the extra deflection degrees-of-freedom. This is achieved by using an appropriate constraint, e.g., for FSDT plate finite elements, the higher-order shear strain terms are set to zero (*constrained anisoparametric* element). The main advantage of anisoparametric elements is that all energy integrations are performed with the full Gaussian quadrature to guarantee variational consistency; furthermore, the resulting consistent load and mass matrices give rise to superior predictions over the comparable reduced integration elements [40,42]. Efficient beam elements based on RZT and anisoparametric interpolations have recently been examined [59,60].

In this paper, six- and three-node, C^0-continuous, RZT-based triangular plate finite elements are developed for the analysis of multilayer composite and sandwich panels. The theory is reviewed first in order to establish a framework for the development of RZT-based finite elements, and to ascertain the predictive capability of the theory for composite and sandwich laminates. The choice of suitable anisoparametric shape functions is then addressed with the specific focus on the shear-locking issues and their consistent resolution within the variational requirements. The unconstrained kinematic field yields a fully-integrated six-node element. To achieve a simple three-node configuration, two different edge-constraint strategies are implemented, giving rise to two distinct three-node triangular elements. Computational studies using thin composite plates are first carried out to verify the free of shear locking behavior for these anisoparametric elements. As a demonstration of shear locking behavior, the fully-integrated, three-node isoparametric (linear interpolation) element is examined. Furthermore, the new anisoparametric elements are examined on several elasto-static problems of moderately thick laminated composite and sandwich plates subjected to different loading and boundary conditions. Excellent convergence characteristics and through-the-thickness predictive capabilities are demonstrated. This paper is an enhanced version of the work presented in [61].

2. REFINED ZIGZAG THEORY FOR PLATES

Herein the basic notation, definitions, and mathematical foundation of the Refined Zigzag Theory (RZT) for plates are reviewed to establish the framework for the

development of RZT-based plate finite elements. For a complete and detailed discussion on RZT for plates, refer to [35-39].
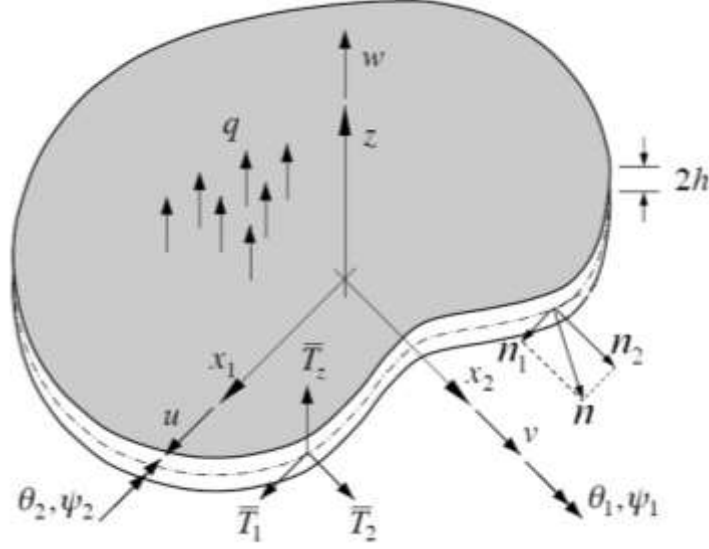

Figure 1. Plate notation.

2.1 Displacements, zigzag kinematics, strains, and stresses

A plate of thickness $2h$ is made of N perfectly bonded orthotropic material layers (Figure 1); the (k) superscript denotes the $k-th$ layer. The plate is referred to a Cartesian coordinate system $(x_1,\ x_2,\ z)$. The middle reference plane (or mid-plane) S_m is denoted by the ordered pair $(x_1,\ x_2) \in S_m$; z is the through-the-thickness coordinate that ranges from $-h$ to h with $z=0$ identifying the mid-plane while the $k-th$ layer thickness is defined in the range $[z_{(k-1)}, z_{(k)}]$, with the first layer beginning at $z_{(0)} = -h$, the last $N-th$ layer ending at $z_{(N)} = h$ (see Figure 2a). S denotes the total cylindrical edge-surface and is composed of $S_u \subset S$, where the displacement restraints are imposed, and of $S_\sigma \subset S$, where external loads may be applied (in our case, a traction vector ($\overline{T}_1, \overline{T}_2, \overline{T}_z$)). The following relations hold: $S_\sigma \cup S_u = S$ and $S_\sigma \cap S_u = \varnothing$. A normal-pressure loading, q, defined as positive in the positive z-direction, is also applied to the mid-plane. The total perimeter surrounding S_m is defined by $C = C_\sigma \cup C_u$ with $C_\sigma = S_\sigma \cap S_m$ and $C_u = S_u \cap S_m$.

6

The RZT displacement components corresponding to the Cartesian coordinate system (x_1, x_2, z) are defined as (refer to [35-37])

$$u_1^{(k)}(x_1, x_2, z) = u(x_1, x_2) + z\theta_1(x_1, x_2) + \phi_1^{(k)}(z)\psi_1(x_1, x_2)$$
$$u_2^{(k)}(x_1, x_2, z) = v(x_1, x_2) + z\theta_2(x_1, x_2) + \phi_2^{(k)}(z)\psi_2(x_1, x_2) \qquad (1)$$
$$u_z^{(k)}(x_1, x_2, z) = w(x_1, x_2)$$

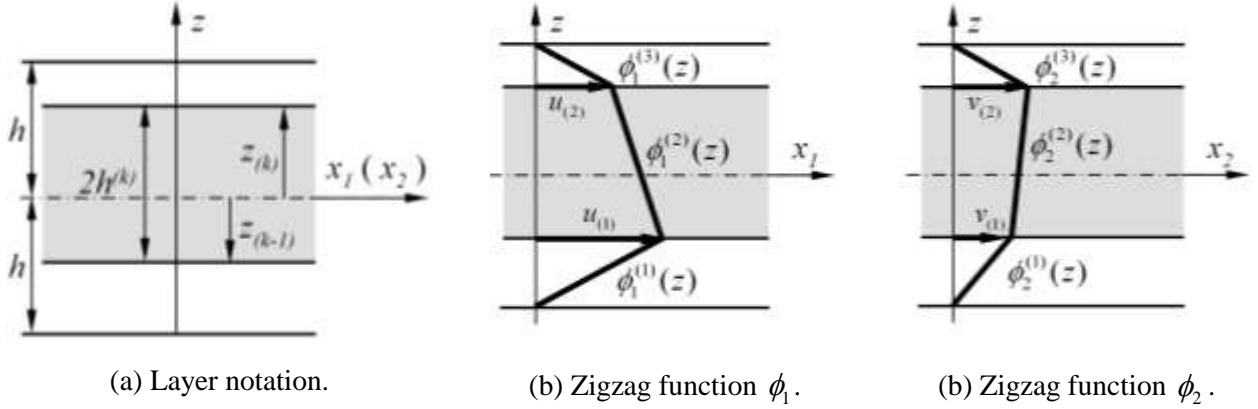(a) Layer notation.   (b) Zigzag function ϕ_1.   (b) Zigzag function ϕ_2.

Figure 2. Layer notation and zigzag functions of the Refined Zigzag Theory for a three-layered laminate

(a) Layer notation. (b) Zigzag function $\boldsymbol{\varphi_1}$. (c) Zigzag function φ_2.

where u, v, and w are the uniform displacement components along the x_1, x_2, and z-axis respectively (u and v are the in-plane displacements while w is the transverse deflection); θ_1 and θ_2 are the average rotations of the transverse normal around the positive x_2-axis and the negative x_1-axis, respectively; and ψ_α $(\alpha = 1,2)$ are the amplitudes of the zigzag contributions to the in-plane displacement in the x_α-directions (Figure 1). Thus, RZT has seven kinematic variables – two more than FSDT; in vector form they are defined as $\mathbf{u} = [u \quad v \quad w \quad \theta_1 \quad \theta_2 \quad \psi_1 \quad \psi_2]^T$.

The zigzag terms $\phi_\alpha^{(k)}(z)\psi_\alpha(x_1, x_2)$ $(\alpha = 1,2)$ in Eq. (1) describe cross-sectional distortions in the form of C^0-continuous piecewise patterns that are typical of multilayer laminates. The zigzag functions, $\phi_\alpha^{(k)}(z)$, have units of length and are piecewise linear, C^0-continuous functions of the thickness coordinate z and, as will be shown subsequently, they are also lamination and material dependent.

It is convenient to define $\phi_1^{(k)}(z)$ and $\phi_2^{(k)}(z)$ in terms of their layer-interface values, $u_{(i)}$ and $v_{(i)}$ $(i = 0, 1, ..., N)$, respectively, so that the homogeneous conditions on the top and bottom surfaces are identically satisfied (refer to Figures 2b and 2c which show the notation for a three-layered laminate), i.e.,

$$
\begin{aligned}
u_{(0)} = \phi_1^{(1)}(-h) = 0, \quad u_{(N)} = \phi_1^{(N)}(+h) = 0 \\
v_{(0)} = \phi_2^{(1)}(-h) = 0, \quad v_{(N)} = \phi_2^{(N)}(+h) = 0
\end{aligned}
\tag{2}
$$

The interior interface values of the zigzag functions are defined as follows

$$
\left.
\begin{aligned}
u_{(k)} = u_{(k-1)} + 2h^{(k)} \beta_1^{(k)} \\
v_{(k)} = v_{(k-1)} + 2h^{(k)} \beta_2^{(k)}
\end{aligned}
\right\} \quad (k = 1, ..., N-1)
\tag{3}
$$

with

$$
\beta_\alpha^{(k)} \equiv \phi_{\alpha,z}^{(k)} = \frac{G_\alpha}{Q_{\alpha\alpha}^{(k)}} - 1 \quad (\alpha = 1, 2; \ k = 1, ..., N-1)
\tag{4}
$$

where $(\cdot)_{,\alpha} \equiv \partial(\cdot)/\partial x_\alpha$ denotes partial differentiation and where G_1 and G_2 are weighted-average transverse-shear stiffness coefficients of their respective lamina-level coefficients, $Q_{11}^{(k)}$ and $Q_{22}^{(k)}$ (Eq. (8))

$$
G_\alpha = \left(\frac{1}{2h} \sum_{k=1}^{N} \frac{2h^{(k)}}{Q_{\alpha\alpha}^{(k)}} \right)^{-1} \quad (\alpha = 1, 2)
\tag{5a}
$$

Within the $k-th$ material layer the zigzag functions are given as

$$
\begin{aligned}
\phi_1^{(k)} \equiv \tfrac{1}{2}\left(1 - \zeta^{(k)}\right) u_{(k-1)} + \tfrac{1}{2}\left(1 + \zeta^{(k)}\right) u_{(k)} \\
\phi_2^{(k)} \equiv \tfrac{1}{2}\left(1 - \zeta^{(k)}\right) v_{(k-1)} + \tfrac{1}{2}\left(1 + \zeta^{(k)}\right) v_{(k)}
\end{aligned}
\tag{5b}
$$

where $\zeta^{(k)}$ is a non-dimensional thickness coordinate defined for each layer

$$\zeta^{(k)} \equiv \left[\left(z - z_{(k-1)}\right)/h^{(k)} - 1\right] \in [-1,1] \quad (k = 1,...,N) \tag{5c}$$

For further details on the derivation of Eqs. (3)–(5b) refer to [36,37].

In the case of homogeneous, single-layer plates, the zigzag functions $\phi_\alpha^{(k)}$ vanish identically; consequently, the displacement field, Eq. (1), reduces to that of Reissner-Mindlin theory [5,62]. Recently, Tessler et. al. [38,39] showed that within RZT, the homogeneous plates should be modeled as laminated plates with infinitesimally slight levels of heterogeneity. By introducing infinitesimally small differences in the transverse shear stiffnesses of the material layers, full advantage of the zigzag kinematics is invoked. This *homogeneous limit* strategy achieves a homogeneous cross-section by forcing the kinematics into infinitesimally small heterogeneous behavior, thus producing highly accurate response predictions, including those for strains and stresses, without the use of shear correction factors.

Using the linear strain-displacement relations, the in-plane and transverse strains become

$$\varepsilon_{11}^{(k)} = u_{,1} + z\theta_{1,1} + \phi_1^{(k)}\psi_{1,1} \tag{6a}$$

$$\varepsilon_{22}^{(k)} = v_{,2} + z\theta_{2,2} + \phi_2^{(k)}\psi_{2,2} \tag{6b}$$

$$\gamma_{12}^{(k)} = u_{,2} + v_{,1} + z(\theta_{1,2} + \theta_{2,1}) + \phi_1^{(k)}\psi_{1,2} + \phi_2^{(k)}\psi_{2,1} \tag{6c}$$

$$\gamma_{\alpha z}^{(k)} = \gamma_\alpha + \beta_\alpha^{(k)}\psi_\alpha \quad (\alpha = 1,2) \tag{6d}$$

where the following notation defining the usual FSDT *shear angles* γ_α is used

$$\gamma_\alpha \equiv w_{,\alpha} + \theta_\alpha \tag{7}$$

The generalized Hooke's law for the $k-th$ orthotropic lamina, whose principal material directions are arbitrary with respect to the mid-plane reference coordinates, $(x_1, x_2) \in S_m$, is written as

$$\begin{Bmatrix} \sigma_{11} \\ \sigma_{22} \\ \tau_{12} \\ \tau_{2z} \\ \tau_{1z} \end{Bmatrix}^{(k)} = \begin{bmatrix} C_{11} & C_{12} & C_{16} & 0 & 0 \\ C_{12} & C_{22} & C_{26} & 0 & 0 \\ C_{16} & C_{26} & C_{66} & 0 & 0 \\ 0 & 0 & 0 & Q_{22} & Q_{12} \\ 0 & 0 & 0 & Q_{12} & Q_{11} \end{bmatrix}^{(k)} \begin{Bmatrix} \varepsilon_{11} \\ \varepsilon_{22} \\ \gamma_{12} \\ \gamma_{2z} \\ \gamma_{1z} \end{Bmatrix}^{(k)} \tag{8}$$

where $C_{ij}^{(k)}$ $(i,j=1,2,6)$ and $Q_{pq}^{(k)}$ $(p,q=1,2)$ are the transformed elastic stiffness coefficients referring to the (x_1, x_2, z) coordinate system and relative to the plane-stress condition that ignores the transverse-normal stress. The expression of these coefficients, in terms of the material engineering constants, can be found in [3].

2.2 Virtual work principle

The Principle of Virtual Work (PVW) can be employed to derive the Euler-Lagrange equations of equilibrium and the corresponding set of consistent boundary conditions.

Considering the plate shown in Figure 1 and the applied loads, the virtual work principle may be written as follows [37]

$$0 = \int_{S_m} \int_{-h}^{h} (\sigma_{11}^{(k)} \delta\varepsilon_{11}^{(k)} + \sigma_{22}^{(k)} \delta\varepsilon_{22}^{(k)} + \tau_{12}^{(k)} \delta\gamma_{12}^{(k)} + \tau_{1z}^{(k)} \delta\gamma_{1z}^{(k)} + \tau_{2z}^{(k)} \delta\gamma_{2z}^{(k)}) dz dS +$$
$$- \int_{S_m} q \delta w dS - \int_{C_\sigma} \int_{-h}^{h} [\overline{T}_1 \delta u_1^{(k)} + \overline{T}_2 \delta u_2^{(k)} + \overline{T}_z \delta u_z^{(k)}] dz ds \tag{9}$$

where δ is the variational operator. Substituting Eqs. (1),(6)-(8) in (9) and integrating across the plate thickness, yields the two-dimensional statement of virtual work

$$0 = \int_{S_m} \Big[N_1 \delta u_{,1} + N_2 \delta v_{,2} + N_{12}(\delta u_{,2} + \delta v_{,1})$$
$$+ M_1 \delta\theta_{1,1} + M_2 \delta\theta_{2,2} + M_{12}(\delta\theta_{1,2} + \delta\theta_{2,1}) + Q_1(\delta w_{,1} + \delta\theta_1) + Q_2(\delta w_{,2} + \delta\theta_2) - q\delta w$$
$$+ M_1^\phi \delta\psi_{1,1} + M_2^\phi \delta\psi_{2,2} + M_{12}^\phi \delta\psi_{1,2} + M_{21}^\phi \delta\psi_{2,1} + Q_1^\phi \delta\psi_1 + Q_2^\phi \delta\psi_2 \Big] dS$$
$$- \int_{C_\sigma} \Big[\overline{N}_{1n} \delta u + \overline{N}_{2n} \delta v + \overline{Q}_{zn} \delta w + \overline{M}_{1n} \delta\theta_1 + \overline{M}_{2n} \delta\theta_2 + \overline{M}_{1n}^\phi \delta\psi_1 + \overline{M}_{2n}^\phi \delta\psi_2 \Big] ds \tag{10}$$

In Eq. (10), the membrane stress resultants and conjugate strain measures are [37]

$$\mathbf{N}_m^T \equiv \{N_1, N_2, N_{12}\} \equiv \int_{-h}^{h} \{\sigma_{11}^{(k)}, \sigma_{22}^{(k)}, \tau_{12}^{(k)}\} dz \qquad (11a)$$

$$\mathbf{e}_m^T \equiv \{u_{,1}, \quad v_{,2}, \quad u_{,2} + v_{,1}\} \qquad (11b)$$

The bending stress resultants and conjugate strain measures are [37]

$$\mathbf{M}_b^T \equiv \{M_1, \quad M_1^\phi, \quad M_2, \quad M_2^\phi, \quad M_{12}, \quad M_{12}^\phi, \quad M_{21}^\phi\}$$
$$\equiv \int_{-h}^{h} \{z\sigma_{11}^{(k)}, \quad \phi_1^{(k)}\sigma_{11}^{(k)}, \quad z\sigma_{22}^{(k)}, \quad \phi_2^{(k)}\sigma_{22}^{(k)}, \quad z\tau_{12}^{(k)}, \quad \phi_1^{(k)}\tau_{12}^{(k)}, \phi_2^{(k)}\tau_{12}^{(k)}\} dz \qquad (12a)$$

$$\mathbf{e}_b^T \equiv \{\theta_{1,1}, \quad \psi_{1,1}, \quad \theta_{2,2}, \quad \psi_{2,2}, \quad \theta_{1,2} + \theta_{2,1}, \quad \psi_{1,2}, \quad \psi_{2,1}\} \qquad (12b)$$

The transverse shear stress resultants and conjugate strain measures are [37]

$$\mathbf{Q}_s^T \equiv \{Q_2, \quad Q_2^\phi, \quad Q_1, \quad Q_1^\phi\} \equiv \int_{-h}^{h} \{\tau_{2z}^{(k)}, \quad \beta_2^{(k)}\tau_{2z}^{(k)}, \quad \tau_{1z}^{(k)}, \quad \beta_1^{(k)}\tau_{1z}^{(k)}\} dz \qquad (13a)$$

$$\mathbf{e}_s^T \equiv \{w_{,2} + \theta_2, \quad \psi_2, \quad w_{,1} + \theta_1, \quad \psi_1\} \qquad (13b)$$

Zigzag bending moments, $M_1^\phi, M_2^\phi, M_{12}^\phi, M_{21}^\phi$, and transverse shear forces, Q_2^ϕ, Q_1^ϕ, may be considered as higher-order stress resultants associated with the zigzag term of the in-plane displacements, see Eqs. (1) and (6). The force and moment resultants, due to the prescribed tractions $(\bar{T}_1, \bar{T}_2, \bar{T}_z)$, have the form

$$\{\bar{N}_{1n}, \quad \bar{N}_{2n}, \quad \bar{Q}_{zn}, \quad \bar{M}_{1n}, \quad \bar{M}_{2n}, \quad \bar{M}_{1n}^\phi, \quad \bar{M}_{2n}^\phi\}$$
$$\equiv \int_{-h}^{h} \{\bar{T}_1, \quad \bar{T}_2, \quad \bar{T}_z, \quad z\bar{T}_1, \quad z\bar{T}_2, \quad \phi_1^{(k)}\bar{T}_1, \quad \phi_2^{(k)}\bar{T}_2\} dz \qquad (14)$$

Integrals across the plate thickness defining resultant forces and moments, Eqs. (11a),(12a),(13a),(14), may be also expressed in terms of summations over the N layers

$$\int_{-h}^{h} f^{(k)}(z) dz = \sum_{k=1}^{N} \left(\int_{z_{(k-1)}}^{z_{(k)}} f^{(k)}(z) dz \right)$$

11

The resulting constitutive relations of the RZT for plates are expressed in matrix form as

$$\begin{Bmatrix} \mathbf{N_m} \\ \mathbf{M_b} \\ \mathbf{Q_s} \end{Bmatrix} = \begin{bmatrix} \mathbf{A} & \mathbf{B} & \mathbf{0} \\ \mathbf{B^T} & \mathbf{D} & \mathbf{0} \\ \mathbf{0} & \mathbf{0} & \mathbf{G} \end{bmatrix} \begin{Bmatrix} \mathbf{e_m} \\ \mathbf{e_b} \\ \mathbf{e_s} \end{Bmatrix} \equiv \mathbf{R}\,\boldsymbol{\omega} \tag{15}$$

where the stiffness matrices are defined as [37]

$$\begin{aligned} \mathbf{A} &\equiv \int_{-h}^{h} \mathbf{C}^{(k)} dz \\ \mathbf{B} &\equiv \int_{-h}^{h} \mathbf{C}^{(k)} \mathbf{B}_{\phi}^{(k)} dz \\ \mathbf{D} &\equiv \int_{-h}^{h} \mathbf{B}_{\phi}^{(k)T} \mathbf{C}^{(k)} \mathbf{B}_{\phi}^{(k)} dz \\ \mathbf{G} &\equiv \int_{-h}^{h} \mathbf{B}_{\beta}^{(k)T} \mathbf{Q}^{(k)} \mathbf{B}_{\beta}^{(k)} dz \end{aligned} \tag{16}$$

with

$$\mathbf{C}^{(k)} \equiv \begin{bmatrix} C_{11} & C_{12} & C_{16} \\ C_{12} & C_{22} & C_{26} \\ C_{16} & C_{26} & C_{66} \end{bmatrix}^{(k)}, \qquad \mathbf{Q}^{(k)} \equiv \begin{bmatrix} Q_{22} & Q_{12} \\ Q_{12} & Q_{11} \end{bmatrix}^{(k)}$$

$$\mathbf{B}_{\phi}^{(k)} \equiv \begin{bmatrix} z & \phi_1^{(k)} & 0 & 0 & 0 & 0 & 0 \\ 0 & 0 & z & \phi_2^{(k)} & 0 & 0 & 0 \\ 0 & 0 & 0 & 0 & z & \phi_1^{(k)} & \phi_2^{(k)} \end{bmatrix}, \quad \mathbf{B}_{\beta}^{(k)} \equiv \begin{bmatrix} 1 & \beta_2^{(k)} & 0 & 0 \\ 0 & 0 & 1 & \beta_1^{(k)} \end{bmatrix} \tag{17}$$

Performing the integration by parts in Eq. (10) results in the Euler-Lagrange equilibrium equations

$$\begin{aligned} \delta u: \quad & N_{1,1} + N_{12,2} = 0 & \delta v: \quad & N_{12,1} + N_{2,2} = 0 & \delta w: \quad & Q_{1,1} + Q_{2,2} + q = 0 \\ \delta\theta_1: \quad & M_{1,1} + M_{12,2} - Q_1 = 0 & \delta\theta_2: \quad & M_{12,1} + M_{2,2} - Q_2 = 0 \\ \delta\psi_1: \quad & M_{1,1}^{\phi} + M_{12,2}^{\phi} - Q_1^{\phi} = 0 & \delta\psi_2: \quad & M_{21,1}^{\phi} + M_{2,2}^{\phi} - Q_2^{\phi} = 0 \end{aligned} \tag{18}$$

and the set of consistent geometric (kinematic-variable) and kinetic (stress-resultant) boundary conditions on the mid-plane perimeter C

$$
\begin{array}{llllll}
u = \bar{u} & on \ C_u & or & N_1 \, n_1 + N_{12} \, n_2 = \bar{N}_{1n} & on \ C_\sigma \\
v = \bar{v} & on \ C_u & or & N_{12} \, n_1 + N_2 \, n_2 = \bar{N}_{2n} & on \ C_\sigma \\
w = \bar{w} & on \ C_u & or & Q_1 \, n_1 + Q_2 \, n_2 = \bar{Q}_{zn} & on \ C_\sigma \\
\theta_1 = \bar{\theta}_1 & on \ C_u & or & M_1 \, n_1 + M_{12} \, n_2 = \bar{M}_{1n} & on \ C_\sigma \\
\theta_2 = \bar{\theta}_2 & on \ C_u & or & M_{12} \, n_1 + M_2 \, n_2 = \bar{M}_{2n} & on \ C_\sigma \\
\psi_1 = \bar{\psi}_1 & on \ C_u & or & M_1^\phi \, n_1 + M_{12}^\phi \, n_2 = \bar{M}_{1n}^\phi & on \ C_\sigma \\
\psi_2 = \bar{\psi}_2 & on \ C_u & or & M_{21}^\phi \, n_1 + M_2^\phi \, n_2 = \bar{M}_{2n}^\phi & on \ C_\sigma
\end{array}
\tag{19}
$$

where the unit outward normal vector to the mid-plane boundary is defined by the direction cosines $\mathbf{n} \equiv [n_1, n_2] = [\cos(x_1, n), \cos(x_2, n)]$, see Figure 1.

The two-dimensional variational statement, Eq. (10), can now be used to derive suitable plate finite elements. Since the strain quantities in the variational statement do not exceed the first spatial derivatives of the kinematic variables, C^0-continuous shape functions may be used to derive kinematically compatible elements.

3. PLATE ELEMENT FORMULATION

Once the kinematic variables are approximated using suitable shape functions, the virtual work principle, Eq. (10), can be used to derive the element-level equilibrium equations; they consist of the element stiffness matrix and load vector.

Next, the choices of suitable shape functions for RZT-based triangular elements are discussed. In particular, the initial attention is on the *shear-locking* phenomenon and its consistent resolution within the use of anisoparametric shape functions and full-order integration of all strain energy terms. For a similar discussion pertaining to the RZT-based beam bending elements, the reader is referred to [60].

3.1 Shear locking and shape functions

The RZT strain definitions, Eqs. (6), contain first derivatives of the kinematic unknowns u, v, w, θ_1, θ_2, ψ_1, and ψ_2. The implication is that C^0-continuous shape functions can be used to approximate these unknowns over an element domain. Although highly desirable in terms of computational efficiency and ease of use, the elements based on C^0-continuous approximations may exhibit excessive stiffening (i.e.,

13

shear locking) when modeling very thin beams, plates or shells. This occurs, for example, in the Reissner-Mindlin plate finite elements based on linear, isoparametric shape functions [57].

Although many different strategies have been proposed in the literature to alleviate the detrimental effects of shear locking (see the Introduction and references herein), the *anisoparametric* interpolations pioneered by Tessler and co-workers [43,45,57,58] provide the most consistent and effective way of formulating bending elements of higher accuracy for beam, plate and shell structures [42]. The *anisoparametric* interpolations use shape functions for the deflection variable that are one degree higher than those used for the bending rotations. Having the average shear angle of the same mathematical form, RZT-based elements are also inherently susceptible to shear locking [59,60,63,64]. The anisoparametric interpolation strategy also permits simple, isoparametric-like nodal patterns by invoking element-level constraint conditions on the transverse shear strain measures or forces [60].

3.2 Six-node *unconstrained anisoparametric* element

A six-node triangular plate element based on RZT and anisoparametric interpolations is presented first. Using linear shape functions for the in-plane displacements, bending rotations, and zigzag amplitudes, and a quadratic shape function for the deflection, the element interpolations in terms of the linear area-parametric coordinates L_i [42] are stated as

$$u(x_1, x_2) = \sum_{i=1}^{3} u_i L_i(x_1, x_2) \qquad v(x_1, x_2) = \sum_{i=1}^{3} v_i L_i(x_1, x_2) \qquad w(x_1, x_2) = \sum_{k=1}^{6} w_k P_k(x_1, x_2)$$

$$\theta_1(x_1, x_2) = \sum_{i=1}^{3} \theta_{1i} L_i(x_1, x_2) \qquad \theta_2(x_1, x_2) = \sum_{i=1}^{3} \theta_{2i} L_i(x_1, x_2) \qquad (20)$$

$$\psi_1(x_1, x_2) = \sum_{i=1}^{3} \psi_{1i} L_i(x_1, x_2) \qquad \psi_2(x_1, x_2) = \sum_{i=1}^{3} \psi_{2i} L_i(x_1, x_2)$$

where $i = 1, 2, 3$ is an index ranging over the three corner nodes; $k = 1, m_{12}, 2, m_{23}, 3, m_{31}$ ranges over the corner and mid-edge nodes; and P_k defines the quadratic shape functions that are also expressed in terms of L_i (see Figure 3.)

In compact matrix form, Eq. (20) can be stated as

$$\mathbf{u} = \mathbf{N}\mathbf{u}^{\mathbf{e}} \qquad (21)$$

where $\mathbf{N}$ is a matrix containing the shape functions, and $\mathbf{u}^{\mathbf{e}}$ is the nodal dof vector; $\mathbf{N}$ and $\mathbf{u}^{\mathbf{e}}$ are defined as

$$\mathbf{N} \equiv \begin{bmatrix} [L_i] & \mathbf{0} & \mathbf{0} & \mathbf{0} & \mathbf{0} & \mathbf{0} & \mathbf{0} \\ \mathbf{0} & [L_i] & \mathbf{0} & \mathbf{0} & \mathbf{0} & \mathbf{0} & \mathbf{0} \\ \mathbf{0} & \mathbf{0} & [P_k] & \mathbf{0} & \mathbf{0} & \mathbf{0} & \mathbf{0} \\ \mathbf{0} & \mathbf{0} & \mathbf{0} & [L_i] & \mathbf{0} & \mathbf{0} & \mathbf{0} \\ \mathbf{0} & \mathbf{0} & \mathbf{0} & \mathbf{0} & [L_i] & \mathbf{0} & \mathbf{0} \\ \mathbf{0} & \mathbf{0} & \mathbf{0} & \mathbf{0} & \mathbf{0} & [L_i] & \mathbf{0} \\ \mathbf{0} & \mathbf{0} & \mathbf{0} & \mathbf{0} & \mathbf{0} & \mathbf{0} & [L_i] \end{bmatrix} \qquad (22)$$

$$\mathbf{u}^{e} \equiv \left[\{u_i\}^T \quad \{v_i\}^T \quad \{w_k\}^T \quad \{\theta_{1i}\}^T \quad \{\theta_{2i}\}^T \quad \{\psi_{1i}\}^T \quad \{\psi_{2i}\}^T \right]^T \qquad (23)$$

with $i = 1, 2, 3$, $k = 1, m_{12}, 2, m_{23}, 3, m_{31}$, and where $[L_i]$ is a 1x3 matrix of the area-parametric coordinates L_i, $[P_k]$ is a 1x6 matrix of the P_k quadratic shape functions, and $\mathbf{0}$ is a null row vector. The resulting finite element possesses three corner nodes $(1, 2, 3)$, each having seven dof's, and three mid-edge nodes (m_{12}, m_{23}, m_{31}) at which only the deflection dof's reside, for a total of twenty four dof's (Figure 3). This *unconstrained anisoparametric* element is labeled Ω_0 (refer to Table 1).
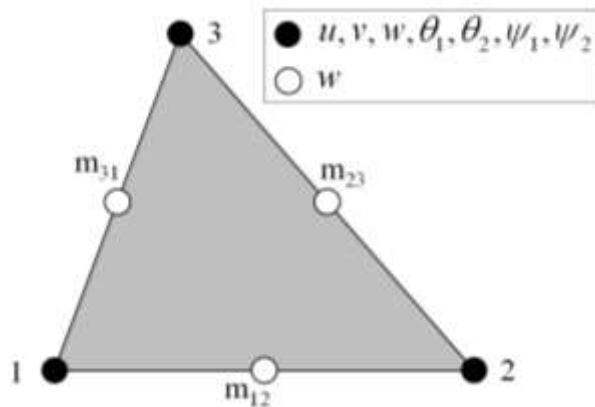

Figure 3. RZT *unconstrained anisoparametric* plate element.

Table 1. Element designation, kinematic interpolation, and nodal configuration.

Type of element	Deflection interpolation	Constraint imposed	No. of nodes (dof's)
Ω_L : Linear isoparametric	Eq. (30): $\alpha = 0$	none	3 (21)
Ω_0 : Unconstrained anisoparametric	Eqs. (20)	none	6 (24)
Ω_γ : Constrained anisoparametric	Eq. (30): $\alpha = 1$, $c = 0$	$\gamma_{nz} = $ const.	3 (21)
Ω_η : Constrained anisoparametric	Eq. (30): $\alpha = 1$, $c = -1$	$\eta_{nz} = $ const.	3 (21)

3.3 Three-node *constrained anisoparametric* elements

The six-node unconstrained anisoparametric element can be slightly reformulated by using continuous edge constraints, leading to a simpler topology and elimination of the mid-edge nodes (Figure 4).

One constraining possibility is that used in FSDT and {1,2}-order anisoparametric elements ([45,57,58]), in which the transverse shear strain γ_{nz} along each element edge (evaluated normally to the edge)

$$\gamma_{nz} \equiv w_{,s} + \theta_n \tag{24}$$

is forced to be constant with respect to the local edge coordinate, s (Figure 5)

$$\frac{\partial \gamma_{nz}}{\partial s} = 0 \tag{25}$$

Yet a different constraining strategy may be undertaken (refer to [59-61,63,64]) by insisting that the second shear-strain measure, which is associated with the zigzag kinematics,

$$\eta_{nz} \equiv \gamma_{nz} - \psi_n \tag{26}$$

be constant along each element edge, i.e.,

$$\frac{\partial \eta_{nz}}{\partial s} = 0 \tag{27}$$

The rotation θ_n and zigzag amplitude ψ_n, oriented along the edge normal, are expressed in terms of the corresponding kinematic variables and angle α_{ij}, as (Figure 5)

$$\theta_n = \theta_1 cos(\alpha_{ij}) + \theta_2 sin(\alpha_{ij})$$
$$\psi_n = \psi_1 cos(\alpha_{ij}) + \psi_2 sin(\alpha_{ij}) \tag{28}$$

Thus, proceeding with the conditions (25) and (27), the mid-edge deflection $w_{m_{ij}}$ is obtained in terms of the dof's at nodes i and j

$$
\begin{aligned}
w_{m_{ij}} ={}& \frac{w_i + w_j}{2} \\
&+ \frac{\left(x_{2j} - x_{2i}\right)}{8}\left[\left(\theta_{1j} + c\psi_{1j}\right) - \left(\theta_{1i} + c\psi_{1i}\right)\right] \\
&+ \frac{\left(x_{1j} - x_{1i}\right)}{8}\left[\left(\theta_{2j} + c\psi_{2j}\right) - \left(\theta_{2i} + c\psi_{2i}\right)\right]
\end{aligned} \tag{29}
$$
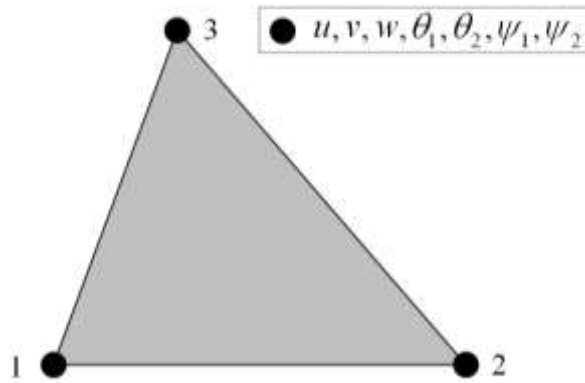
Figure 4. RZT *constrained anisoparametric* plate element.
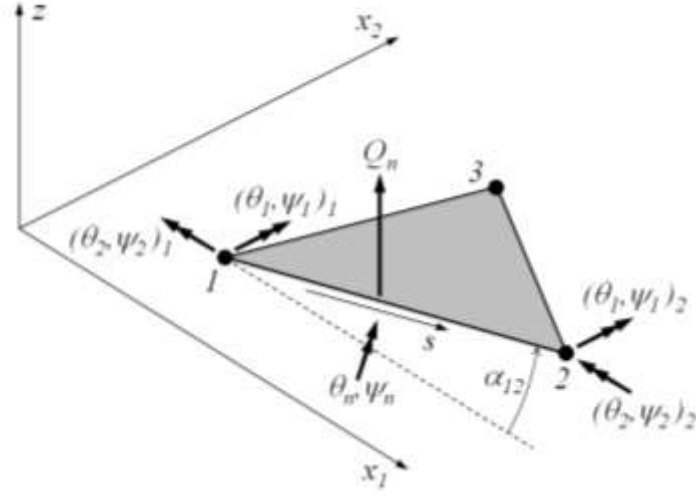
Figure 5. Triangular-element edge definitions of θ_n, ψ_n, Q_n, s and α_{12}.

The transverse-displacement interpolation, Eq. (20), takes on a coupled form

$$w(x_1, x_2) = \sum_{i=1}^{3} L_i w_i + \alpha \sum_{i=1}^{3} \left(\left(\theta_{1i} + c\psi_{1i} \right) L_{1i} + \left(\theta_{2i} + c\psi_{2i} \right) L_{2i} \right) \tag{30}$$

with

$$
\begin{aligned}
L_{1i} &\equiv \frac{L_i}{2} (b_k L_j - b_j L_k) \quad L_{2i} \equiv \frac{L_i}{2} (a_j L_k - a_k L_j) \\
a_i &\equiv x_{1k} - x_{1j} \qquad\qquad b_i \equiv x_{2j} - x_{2k}
\end{aligned}
\tag{31}
$$

where the subscripts are given by the cyclic permutation of $i = 1, 2, 3$, $j = 2, 3, 1$, and $k = 3, 1, 2$. In Eq. (30), α is a flag that permits switching between a linear (α=0, the element is labeled Ω_L, see Table 1) and a parabolic (α=1) approximation of the deflection, and where c is either 0 or -1, depending on the constraining strategy used in the element formulation:

- $c = 0$: γ_{nz} is constant along the three element edges, Eq. (25); the element is labeled Ω_γ (Table 1).

- $c = -1$: η_{nz} is constant along the three element edges, Eq. (27); the Ω_η element.

18

Both the linear isoparametric and constrained anisoparametric elements have three nodes with seven dof's, for a total of twenty one dof's. Eq. (21) remains valid, but with the following definitions of $\mathbf{N}$ and $\mathbf{u^e}$

$$\mathbf{N} \equiv \begin{bmatrix} [L_i] & \mathbf{0} & \mathbf{0} & \mathbf{0} & \mathbf{0} & \mathbf{0} & \mathbf{0} \\ \mathbf{0} & [L_i] & \mathbf{0} & \mathbf{0} & \mathbf{0} & \mathbf{0} & \mathbf{0} \\ \mathbf{0} & \mathbf{0} & [L_i] & \alpha[L_{1i}] & \alpha[L_{2i}] & \alpha c[L_{1i}] & \alpha c[L_{2i}] \\ \mathbf{0} & \mathbf{0} & \mathbf{0} & [L_i] & \mathbf{0} & \mathbf{0} & \mathbf{0} \\ \mathbf{0} & \mathbf{0} & \mathbf{0} & \mathbf{0} & [L_i] & \mathbf{0} & \mathbf{0} \\ \mathbf{0} & \mathbf{0} & \mathbf{0} & \mathbf{0} & \mathbf{0} & [L_i] & \mathbf{0} \\ \mathbf{0} & \mathbf{0} & \mathbf{0} & \mathbf{0} & \mathbf{0} & \mathbf{0} & [L_i] \end{bmatrix} \tag{32}$$

$$\mathbf{u}^e \equiv \left[\{u_i\}^T \quad \{v_i\}^T \quad \{w_i\}^T \quad \{\theta_{1i}\}^T \quad \{\theta_{2i}\}^T \quad \{\psi_{1i}\}^T \quad \{\psi_{2i}\}^T \right]^T \tag{33}$$

with $i = 1, 2, 3$.

Table 1. Element designation, kinematic interpolation, and nodal configuration.

Type of element	Deflection interpolation	Constraint imposed	No. of nodes (dof's)
Ω_L : Linear isoparametric	Eq. (30): $\alpha = 0$	none	3 (21)
Ω_0 : Unconstrained anisoparametric	Eqs. (20)	none	6 (24)
Ω_γ : Constrained anisoparametric	Eq. (30): $\alpha = 1$, $c=0$	$\gamma_{nz} = $ const.	3 (21)
Ω_η : Constrained anisoparametric	Eq. (30): $\alpha = 1$, $c = -1$	$\eta_{nz} = $ const.	3 (21)

3.4 Element stiffness matrix and nodal load vector

Substituting Eq. (21) in Eq. (15) and then in Eq. (10), and after some straightforward operations, the element-level equilibrium equations take on the form

$$\mathbf{K^e u^e} = \mathbf{f^e} \tag{34}$$

The stiffness matrix may be calculated as follows

$$\mathbf{K^e} = \int_{S_m} \mathbf{B^{eT}} \, \mathbf{R} \, \mathbf{B^e} dS \tag{35}$$

where $\mathbf{B^e}$ is the strain-displacement matrix of the element which contains the derivatives of the shape functions with respect to the in-plane coordinates x_1 and x_2, hence $\boldsymbol{\omega} \equiv \mathbf{B^e u^e}$; and $\mathbf{R}$ is the matrix of constitutive properties defined in Eqs. (15)-(17). The $\mathbf{B^e}$ matrices corresponding to the six-node *unconstrained anisoparametric* and three-node *constrained anisoparametric* elements are summarized in the Appendix.

For the case of the transversely distributed loading, $q(x_1,x_2)$, the element consistent load vector, $\mathbf{f^e}$, is defined as

$$\mathbf{f^e} = \int_{S_m} \mathbf{\acute{N}^T} \, q dS \tag{36}$$

where $\mathbf{\acute{N}}$ is composed of the third row of shape-function matrix $\mathbf{N}$, Eqs. (22) or (32).

Finally, to take advantage of the ABAQUS code, the element formulations have been implemented via a user-element subroutine. This allows the user of ABAQUS to invoke a user-defined plate element and relegate the model assembly, application of loading and boundary condition, and problem execution to the ABAQUS code. Furthermore, pre- and post-processing is also carried out using ABAQUS/CAE.

4. NUMERICAL RESULTS

Several numerical results are presented for multilayer composite and sandwich plates, subjected to different loading and boundary conditions, to demonstrate the predictive capabilities of the Refined Zigzag Theory and RZT-based plate finite elements. The numerical results address the following issues: (i) predictive capabilities of RZT over a wide range of material properties and span-to-thickness ratios, (ii) shear locking effects related to the fully-integrated linear element, Ω_L, and the lack of shear locking in the anisoparametric elements, Ω_0, Ω_γ, and Ω_η, and (iii) performance comparisons between the anisoparametric constrained elements, Ω_γ and Ω_η.

4.1 Example problems

Simply supported and cantilevered linear elastic square plates ($a \times a = 20 \times 20 \, cm$) of thickness $2h$ are analyzed over a range of span-to-thickness ratios, $\rho \equiv a/2h$. The following three problems are investigated (refer to Figures 6):

Problem (1): a simply supported plate subjected to the transverse sinusoidal pressure

$$q(x_1, x_2) = q_0 \sin(\pi x_1/a) \sin(\pi x_2/a).$$

Problem (2): a cantilevered plate subjected to the uniform transverse pressure

$$q(x_1, x_2) = q_0.$$

Problem (3): a cantilevered plate subjected to two opposite-direction vertical forces F at the free vertices.

Tables 2 and 3 summarize the mechanical material properties and the laminate stacking sequences, respectively. Laminate A is a symmetric three-layer sandwich plate with orthotropic face-sheets and a PVC core. Laminate B is a non-symmetric three-layer sandwich plate having aluminum face-sheets and an isotropic core with a varying Young's modulus; the core-to-face Young's modulus ratio, $r \equiv E_C / E_F$, ranges from 10^{-5} to 1.

The predictive capabilities of RZT and its finite elements (presented in Sections 3.2 and 3.3) are examined next (refer to Table 1 for the designation of the four finite elements, Ω_L, Ω_0, Ω_γ, and Ω_η.) Whenever available, the results are compared to the exact three-dimensional elasticity or analytic solutions corresponding to the RZT and FSDT theories. The following abbreviations are used to facilitate the discussion of the numerical results:
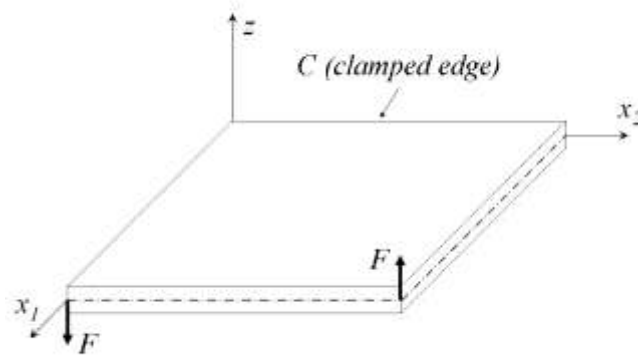
- "Pagano" refers to the exact elasticity solutions for a simply supported laminated plate subjected to a sinusoidal distributed loading (Problem (1), [65]).
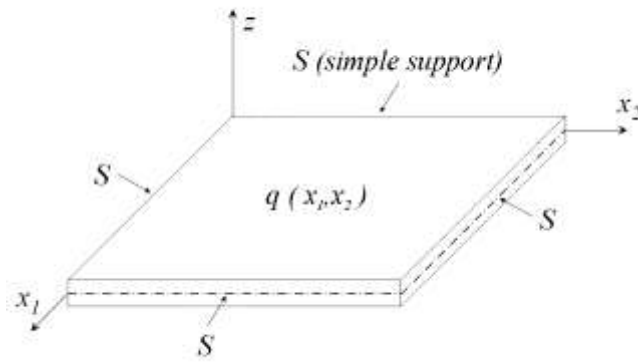
(a) Problem (1)
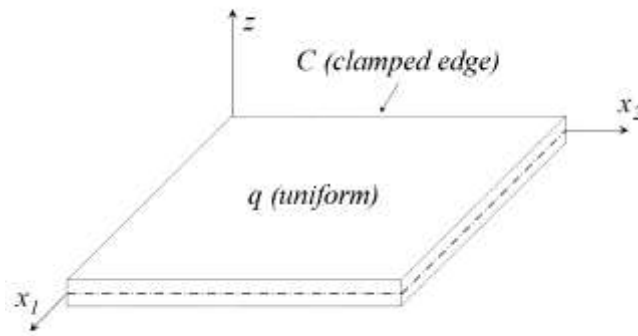
(b) Problem (2)

(c) Problem (3)

Figure 6. Simply supported and cantilevered square plates under transverse loading.

Table 2. Material mechanical properties. The Young's Moduli E and shear moduli G are expressed in GPa.

Orthotropic material		Isotropic materials			
Lamina material	C Carbon-Epoxy	Lamina material	P PVC	A Aluminum	Ar
$E_1^{(k)}$	157.9	$E^{(k)}$	0.104	73	$7.3 \times 10^{-4} - 73$
$E_2^{(k)}$	9.584				
$E_3^{(k)}$	9.584				
$\nu_{12}^{(k)}$	0.32	$\nu^{(k)}$	0.3	0.3	0.3
$\nu_{13}^{(k)}$	0.32				
$\nu_{23}^{(k)}$	0.49				
$G_{12}^{(k)}$	5.930				
$G_{13}^{(k)}$	5.930				
$G_{23}^{(k)}$	3.227				

Table 3. Laminate stacking sequences (the layer sequence is along the positive z direction).

Laminate designation	Thicknesses $\left(2h^{(k)}/2h\right)$	Materials
A	(0.10/0.80/0.10)	(C/P/C)
B	(0.10/0.70/0.20)	(A/Ar/A)

- "RZT" refers to the analytic solutions based on RZT. The solutions for Problem (1) are obtained using suitable trigonometric functions. The solutions for Problem (2) are based on the Rayleigh-Ritz method in which the kinematic variables are approximated using the Gram-Schmidt polynomials (seven functions along the x_1 axis and five along the x_2 axis, [36]).

(a) 2x2 regular mesh (n^e=2).

(b) 4x4 regular mesh (n^e=4).

(c) 2x2 irregular mesh (n^e=2).

(d) 4x4 irregular mesh (n^e=4).
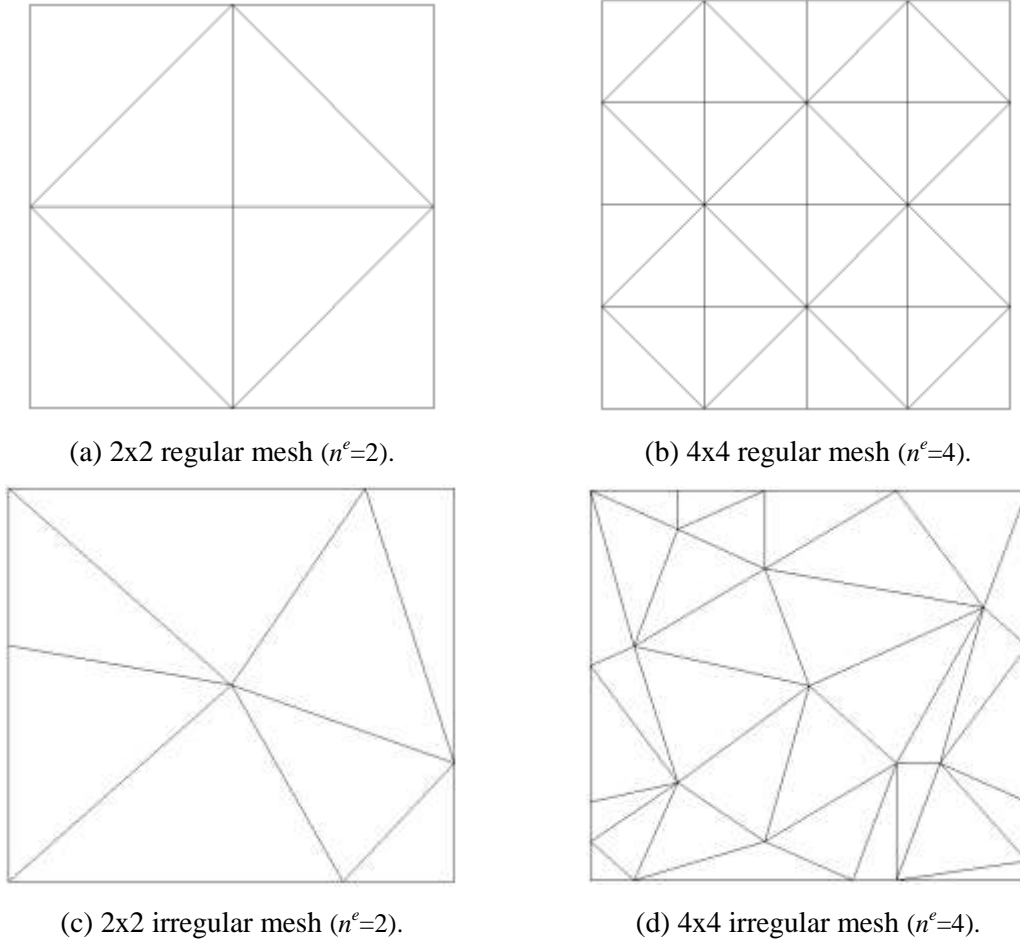
Figure 7. Finite element plate discretizations, regular and irregular.

- "FSDT" refers to the analytic solutions for Problem (1) based on FSDT with trigonometric-function descriptions of the kinematic variables and the $k_1^2 = k_2^2 = 5/6$ shear correction factors.

The finite element solutions are obtained using regular or irregular mesh patterns depicted in Figure 7. The discretizations have the same number of subdivisions along the four plate edges, n^e. Moreover, a node at the plate center, $(x_1, x_2) = (a/2, a/2)$, is always present. When irregular meshes are used, the notation for the finite elements is accompanied by the D superscript, for example Ω_γ^D (see Figure 19).
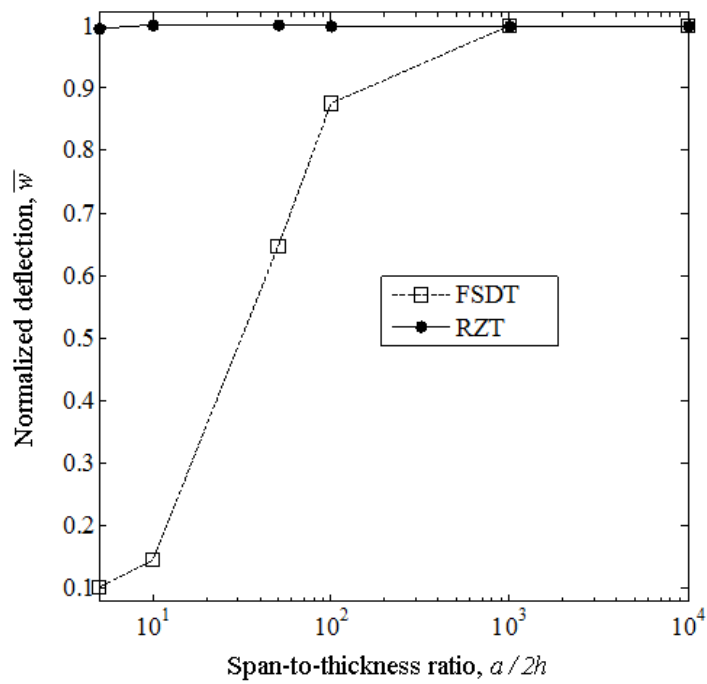
Figure 8. Normalized center deflection, $\bar{w} \equiv w / w^{Pagano}$, vs. span-to-thickness ratio (Problem (1), Laminate A).
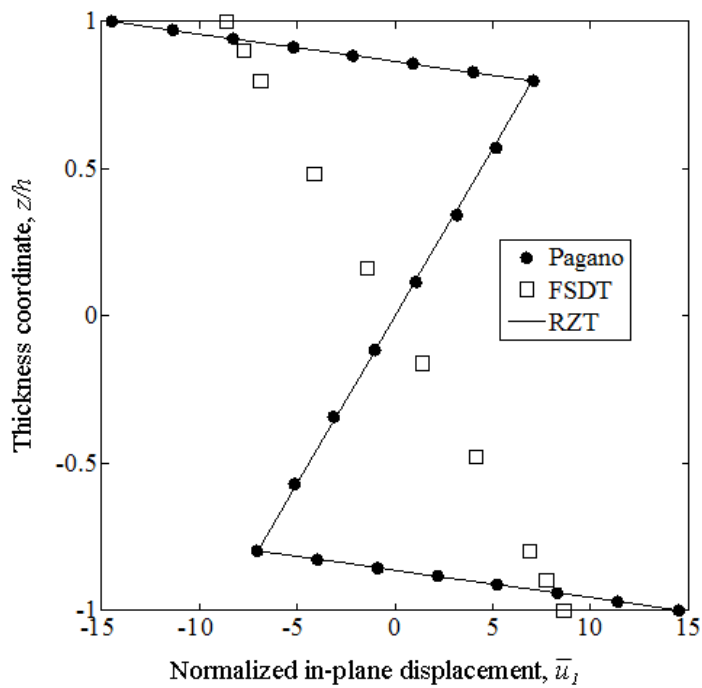
Figure 9. Through-the-thickness distribution of normalized in-plane displacement, $\bar{u}_1 \equiv u_1^{(k)}(a/4, a/2) \times (10^4 D_{11} / q_0 a^4)$ (Problem (1), Laminate A, $a/2h = 10$).

Unless indicated otherwise, the regular meshes are used.

4.2 Results and discussion

Figures 8-12 depict a set of results for Problem (1), for the stacking sequences A and B, that compare the RZT and FSDT predictive capabilities, where Pagano's exact elasticity solutions are used as the reference solutions. In Figures 8 and 12, deflection results are presented, whereas in Figures 9-11, through-the-thickness distributions of the inplane displacement, inplane-normal stress and transverse-shear stress are shown, respectively. The results in Figure 8 demonstrate that, for thick sandwich-like laminates, FSDT underestimates the maximum deflection significantly, whereas the RZT predictions are excellent for the entire range of span-to-thickness ratios examined. The results in Figure 9 demonstrate the superior modeling capability of RZT which predicts accurately the zigzag through-the-thickness distribution of the inplane displacement, whereas FSDT is unable to describe this behavior.
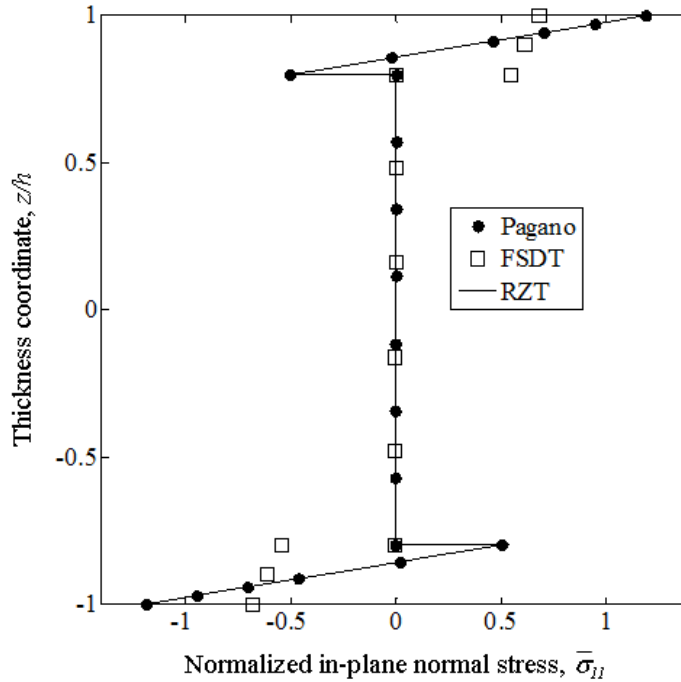
Figure 10. Through-the-thickness distribution of normalized in-plane normal stress, $\bar{\tau}_{1z} \equiv \tau_{1z}^{(k)}(a/4, a/2) \times (1/q_0\rho)$ (Problem (1), Laminate A, $a/2h = 10$).
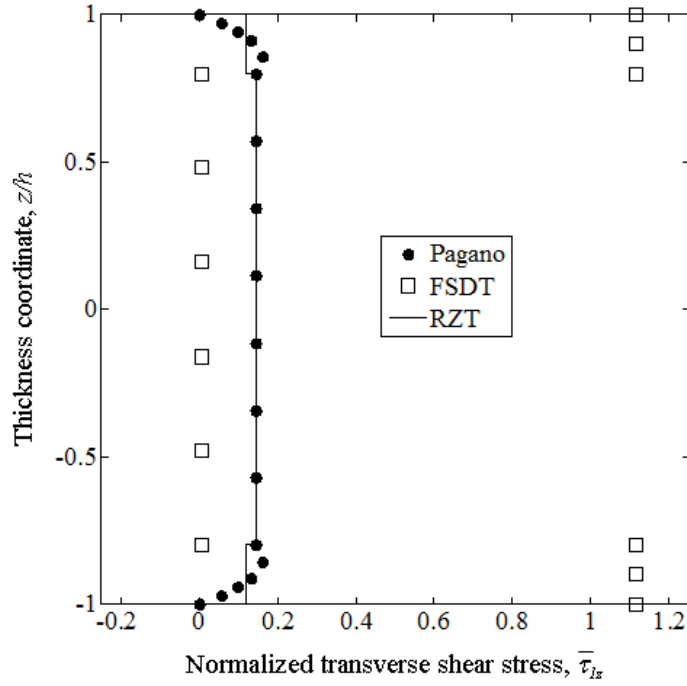
Figure 11. Through-the-thickness distribution of normalized transverse shear stress,

$$\bar{\tau}_{1z} \equiv \tau_{1z}^{(k)}(a/4, a/2) \times (1/q_0\rho) \quad \text{(Problem (1), Laminate A, } a/2h = 10 \text{)}.$$

Consequently, as evidenced from Figure 10, application of RZT results in an accurate description of the inplane normal stress distribution, whereas the FSDT prediction underestimates the maximum stress by approximately 50%. It is shown in Figure 11 that both RZT and FSDT produce piecewise constant through-the-thickness distributions of the transverse shear stress. For this stress component, RZT gives rise to an acceptable approximation of the average stress in each layer, whereas FSDT overestimates the face-sheet values and underestimates the stress in the core region. Additional conclusions can be made from Figure 12, where the normalized deflection of a sandwich plate with a varying core-to-face Young's modulus ratio is shown: while RZT is accurate over the entire range of the examined transverse anisotropy, FSDT underestimates the maximum deflection significantly when the core layer is relatively compliant.
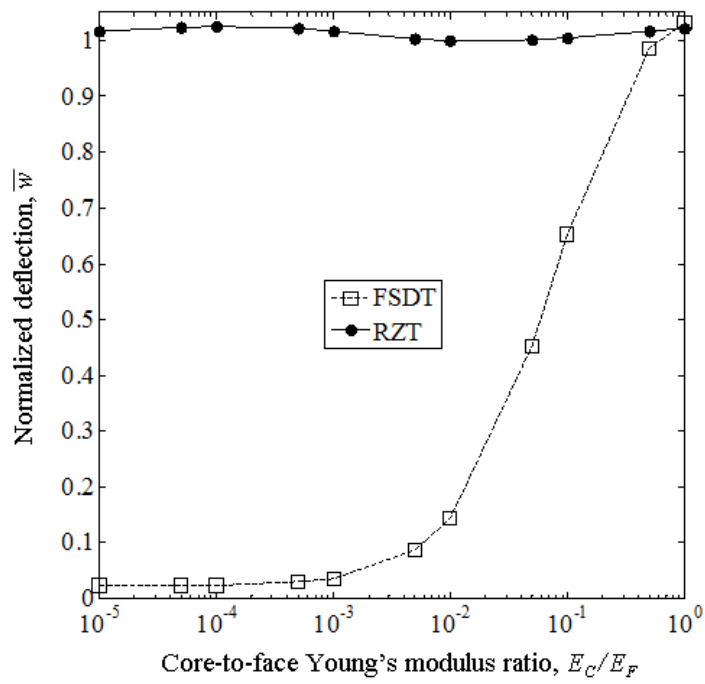
27

Figure 12. Normalized center deflection, $\bar{w} \equiv w/w^{Pagano}$, vs. core-to-face Young's modulus ratio (Problem (1), Laminate B, $a/2h = 5$).
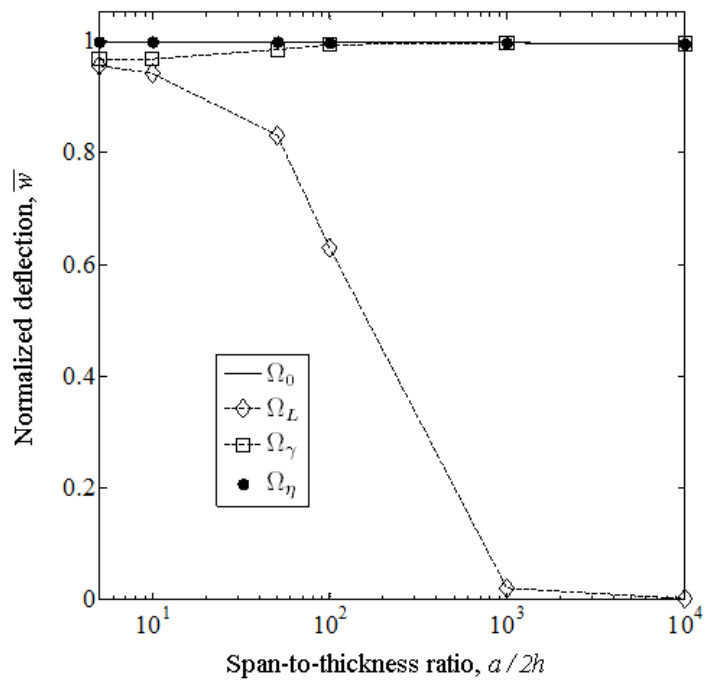

Figure 13. Normalized center deflection, $\bar{w} \equiv w/w^{RZT}$, vs. span-to-thickness ratio (Problem (1), Laminate A, $n^e = 16$).

28

To ascertain if the RZT-based finite elements suffer from shear locking, the deflection predictions for Problem (1) (laminate A) are examined over a range of $a/2h$ ratio, where the analysis is carried out using the $n^e = 16$ regular mesh. As shown in Figure 13, the fully-integrated linear element, Ω_L, exhibits severe shear locking - the deflection decreases significantly as the laminate becomes progressively thinner. On the other hand, the elements based on the anisoparametric interpolations (constrained or unconstrained) do not suffer from this shortcoming and are accurate for both thick and thin plates.

The results in Figures 14-18 correspond to Problem (2) in which a thick laminate ($a/2h=5$) with the stacking sequence A is considered. Figures 14-16 depict convergence plots for the deflection, inplane normal and transverse-shear stresses, where only the regular meshes ranging from $n^e = 2$ to $n^e = 64$ are used (see Figures 7(a) and 7(b)). As expected, the deflection (Figure 14) converges faster than the stresses (Figures 15 and 16).
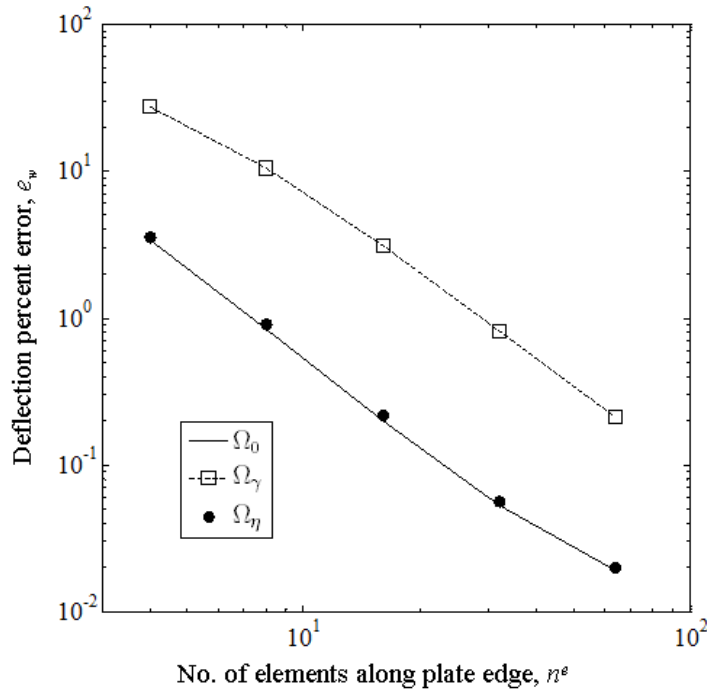

Figure 14. Deflection percent error, $e_w \equiv 100\left(w(a,a/2) - w^{RZT}(a,a/2)\right)\big/w^{RZT}(a,a/2)$, vs. number of elements along plate edge (Problem (2), Laminate A, $a/2h = 5$).
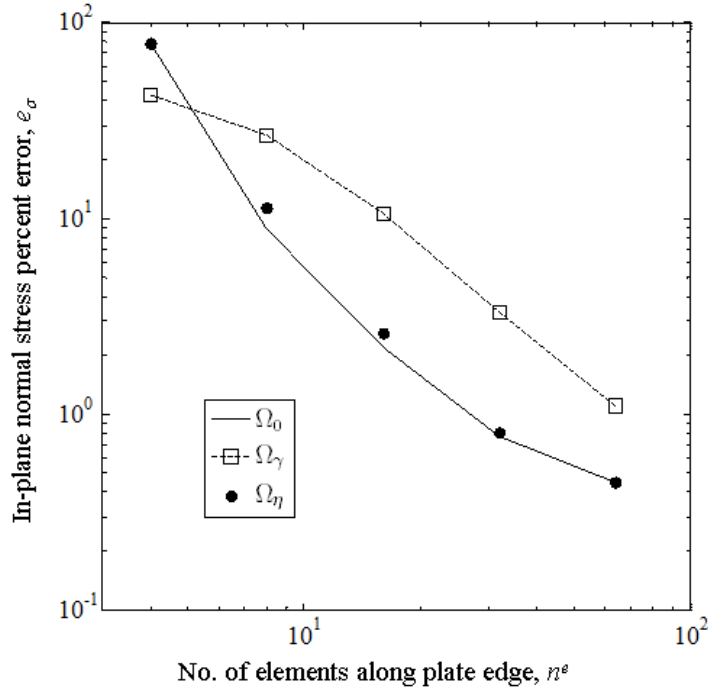
Figure 15. In-plane normal stress percent error,

$$e_\sigma \equiv 100\left(\sigma_{11}^{(3)}\left(a/4,a/2,h\right) - \sigma_{11}^{(3)RZT}\left(a/4,a/2,h\right)\right)\Big/\sigma_{11}^{(3)RZT}\left(a/4,a/2,h\right),$$ vs. number of elements

along plate edge (Problem (2), Laminate A, $a/2h = 5$).

These results also reveal that the Ω_0 unconstrained element is the most accurate of all elements examined. The Ω_η constrained element ($\eta_{nz} = const.$) is slightly less accurate, whereas the Ω_γ ($\gamma_{nz} = const.$) constrained element exhibits somewhat inferior accuracy. In Figures 17 and 18, through-the-thickness distributions of the inplane normal and transverse-shear stresses are depicted, where the Ω_0 element results for $n^e = 8$ and 16 are compared with the corresponding analytic solutions of RZT. Herein, the finite element stresses were evaluated at a node located at $(x_1, x_2) = (a/4, a/2)$, by averaging the four stress values computed at the centroid of each of the four elements that share that node. It is seen from the figures that the Ω_0 predictions are in excellent agreement with the RZT analytic solutions. Also note that the transverse shear stresses, computed by RZT using Hooke's law, are constant within each layer. These stresses should be regarded as some average representations of their true distributions across the individual layers.
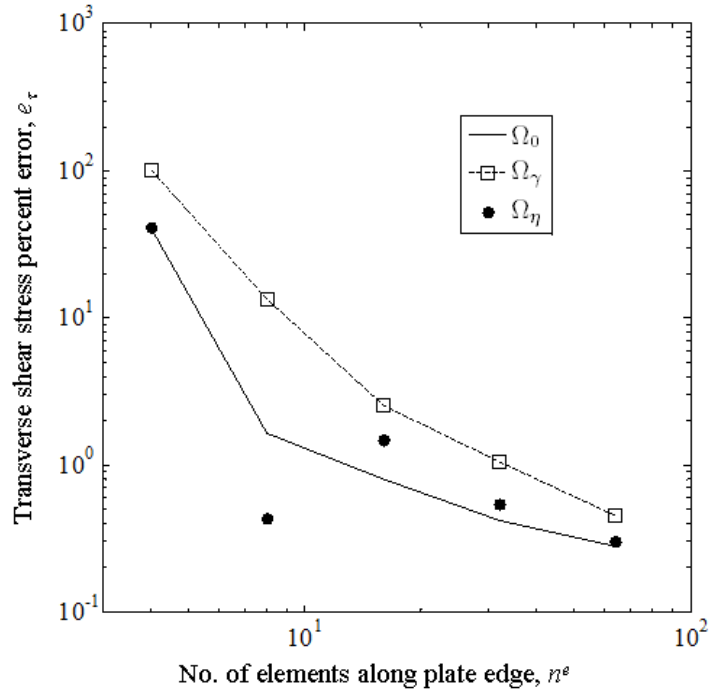
30

Figure 16. Transverse shear stress percent error,

$$e_\tau \equiv 100 \left(\tau_{1z}^{(3)} \left(a/4, a/2 \right) - \tau_{1z}^{(3)RZT} \left(a/4, a/2 \right) \right) \Big/ \tau_{1z}^{(3)RZT} \left(a/4, a/2 \right),\ \text{vs. number of elements along}$$
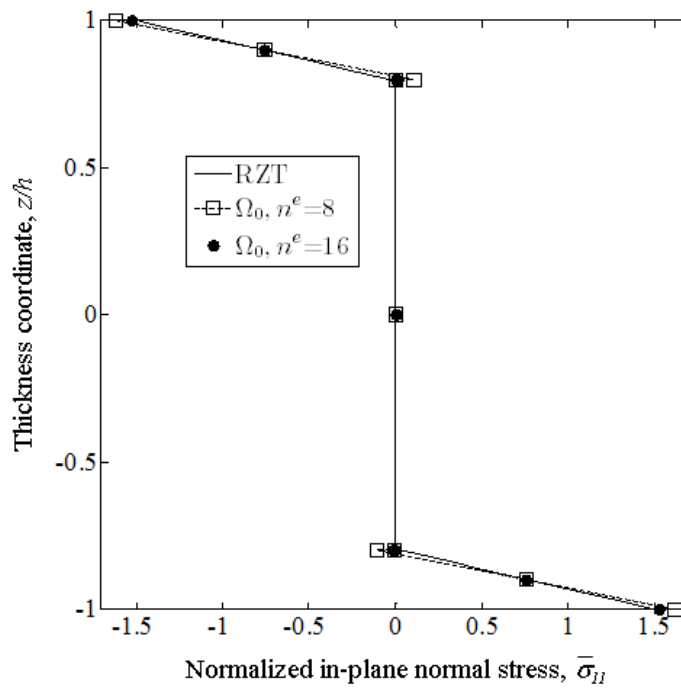
plate edge (Problem (2), Laminate A, $a/2h = 5$).

Figure 17. Through-the-thickness distribution of normalized in-plane normal stress,

$$\bar{\sigma}_{11} \equiv \sigma_{11}^{(k)} (a/4, a/2) \times (1/q_0 \rho^2),\ \text{(Problem (2), Laminate A, } a/2h = 5).$$

Moreover, these average values often provide reasonable approximations for these stresses corresponding to the midplane position through a layer thickness. Therefore, reliable values of the transverse shear stresses at $z = \pm h$ cannot be inferred when Hooke's law is used to compute these stresses, i.e., the stresses will not match exactly the prescribed transverse shear tractions along these boundaries. On the other hand, integration of the equilibrium equations of three-dimensional elasticity theory, involving derivatives of the inplane stresses, generally yields highly accurate results for the transverse shear stresses across the laminate thickness, including those at the bounding surfaces $z = \pm h$. This is because the through-the-thickness distributions of the inplane stresses obtained with RZT are highly accurate (e.g., refer to [36, 37]).

In Figure 19, convergence plots for the deflection are depicted for all element types, including the results for the irregular (distorted) meshes (Ω_γ^D and Ω_η^D, Figures 7(c) and 7(d)), where the results correspond to Problem (1) using a thick laminate ($a/2h=5$) with the stacking
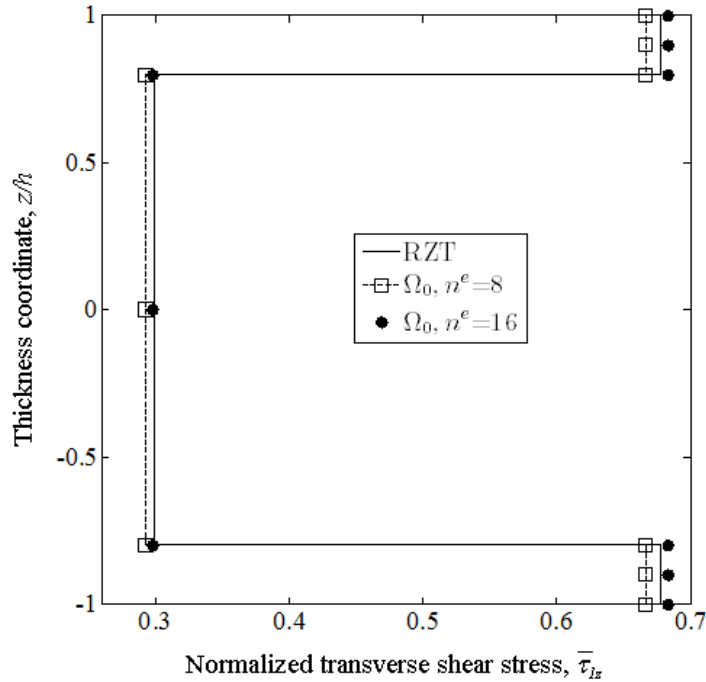

Figure 18. Through-the-thickness distribution of normalized transverse shear stress,
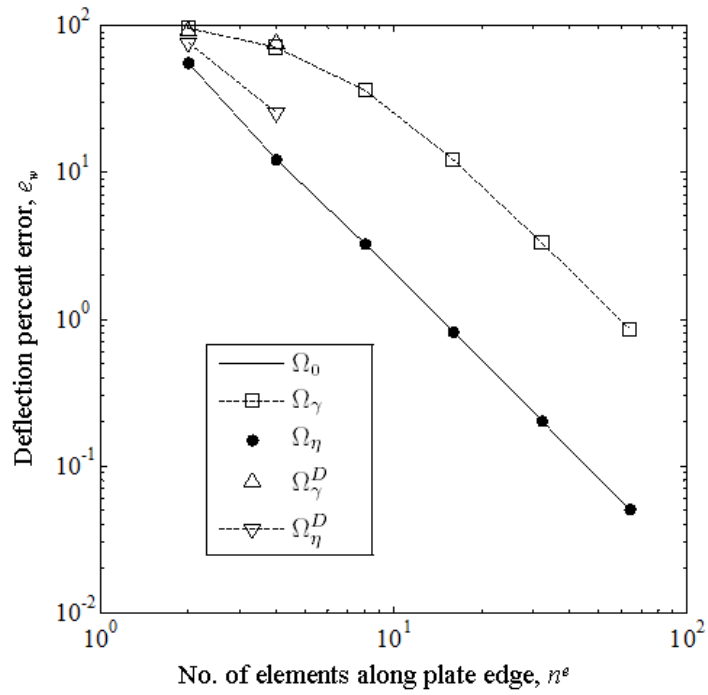$$\bar{\tau}_{1z} \equiv \tau_{1z}^{(k)}(a/4,a/2) \times (1/q_0\rho) \quad \text{(Problem (2), Laminate A, } a/2h=5\text{)}.$$

32

Figure 19. Center deflection percent error, $e_w \equiv 100\left(w - w^{RZT}\right)/w^{RZT}$, vs. number of elements along plate edge (Problem (1), Laminate A, $a/2h = 5$).
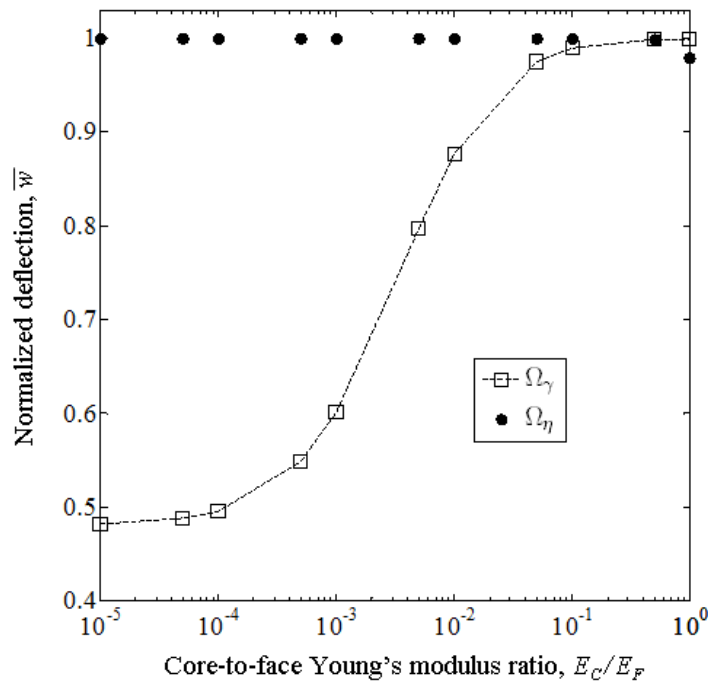
sequence A. It is noted that even the distorted meshes produce highly accurate results using these elements, with the Ω_η element exhibiting superior performance over the Ω_γ element.

 To assess the effect of transverse heterogeneity on the performance of the Ω_η and Ω_γ constrained elements, problems (1), (2), and (3) for thick plates ($a/2h = 5$) with the stacking sequence B are solved using a relatively fine regular mesh of $n^e = 16$. In Figures 20-22, the center deflection is plotted versus the $r = E_C / E_F$ ratio, where the deflection is normalized with respect to the corresponding Ω_0 element predictions. Note that the material ratio $r = E_C / E_F$ signifies a range of laminates, from highly heterogeneous (small r) to nearly homogeneous (r close to 1). As shown in these figures, the Ω_η element predictions are superior for the highly heterogeneous laminates. Conversely, the quasi-homogeneous laminates are modeled somewhat more accurately using the Ω_γ element. Overall, however, the Ω_η element produces superior performance over the range of the r ratio examined.
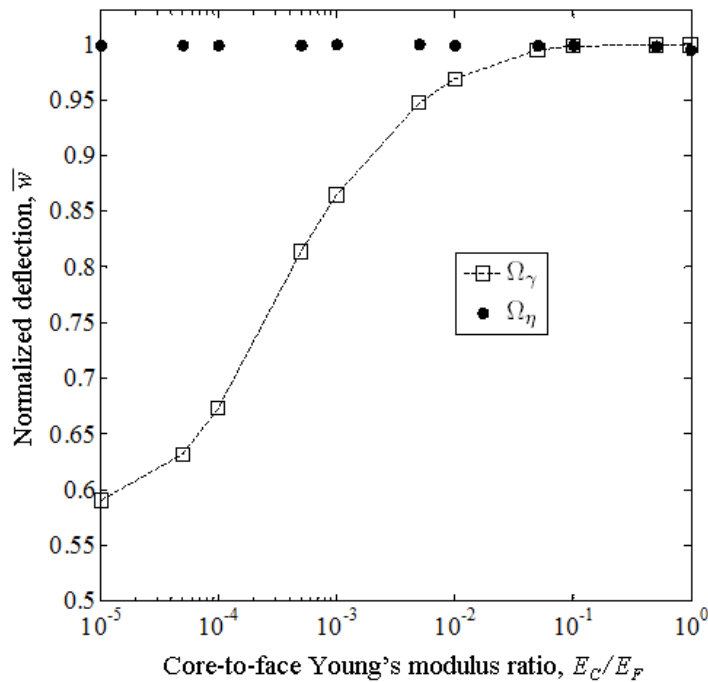
Figure 21. Normalized deflection, $\bar{w} \equiv w(a, a/2) \big/ w^{\Omega_0}(a, a/2)$, vs. core-to-face Young's modulus ratio (Problem (2), Laminate B, $a/2h = 5$, $n^e = 16$).
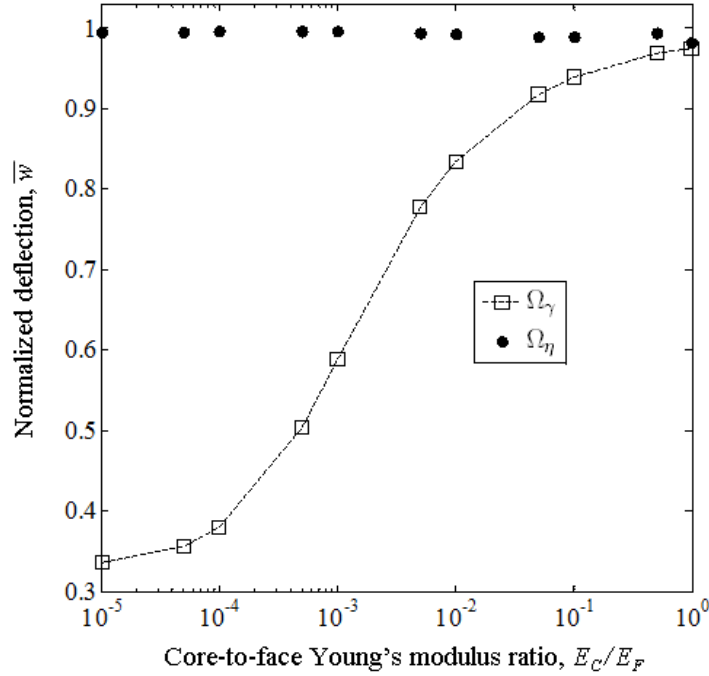

Figure 22. Normalized deflection, $\bar{w} \equiv w(a, a) \big/ w^{\Omega_0}(a, a)$, vs. core-to-face Young's modulus ratio (Problem (3), Laminate B, $a/2h = 5$, $n^e = 16$).

5. CONCLUSIONS

The Refined Zigzag Theory (RZT) for homogeneous, multilayer composite and sandwich plates has been adopted to develop a set of computationally efficient triangular plate elements that use six- and three-node configurations. To guarantee proper element behavior when thin plates are modeled, anisoparametric C^0-continuous shape functions have been adopted to interpolate the element kinematic fields. Full-quadrature integration has been used on all stiffness and load-vector terms to ensure variational consistency and correct stiffness-matrix rank. Starting from the unconstrained anisoparametric interpolations, which give rise to seven kinematic degrees-of-freedom associated with the corner nodes and deflection degrees-of-freedom at the mid-edge nodes, and by imposing continuous constraint conditions on the shear

strain measures along element edges, two distinct three-node constrained anisoparametric elements have been derived.

The elements have been implemented in the ABAQUS commercial finite element code via a user-element subroutine. The three-node elements, based on the constrained deflection interpolations, have shown to provide the best compromise between computational efficiency and accuracy. The numerical studies for simply supported and cantilevered plates undergoing elasto-static deformations have demonstrated that the new RZT-based anisoparametric elements have excellent convergence characteristics over a wide range of the span-to-thickness ratio. Furthermore, they provide superior through-the-thickness predictions when modeling laminated composite plates, including the highly heterogeneous sandwich laminations. This novel element technology offers substantial improvements over the current state-of-the-art plate modeling which is either based on FSDT or higher-order plate and continuum solid elements.

APPENDIX

The strain-displacement $\mathbf{B}^{\mathrm{e}}$ matrix for the six-node, twenty-four-dof *unconstrained anisoparametric* element, Ω_0, is given by

$$
\mathbf{B}^{\mathrm{e}} \equiv
\begin{bmatrix}
[L_{i,x}] & 0 & 0 & 0 & 0 & 0 & 0 \\
0 & [L_{i,y}] & 0 & 0 & 0 & 0 & 0 \\
[L_{i,y}] & [L_{i,x}] & 0 & 0 & 0 & 0 & 0 \\
0 & 0 & 0 & [L_{i,x}] & 0 & 0 & 0 \\
0 & 0 & 0 & 0 & 0 & [L_{i,x}] & 0 \\
0 & 0 & 0 & 0 & [L_{i,y}] & 0 & 0 \\
0 & 0 & 0 & 0 & 0 & 0 & [L_{i,y}] \\
0 & 0 & 0 & [L_{i,y}] & [L_{i,x}] & 0 & 0 \\
0 & 0 & 0 & 0 & 0 & [L_{i,y}] & 0 \\
0 & 0 & 0 & 0 & 0 & 0 & [L_{i,x}] \\
0 & 0 & [P_{k,y}] & 0 & [L_i] & 0 & 0 \\
0 & 0 & 0 & 0 & 0 & 0 & [L_i] \\
0 & 0 & [P_{k,x}] & [L_i] & 0 & 0 & 0 \\
0 & 0 & 0 & 0 & 0 & [L_i] & 0
\end{bmatrix}
\tag{A1}
$$

The $\mathbf{B}^e$ matrix which corresponds to the three-node, twenty-one-dof *constrained anisoparametric* elements, Ω_γ and Ω_η, is given by

$$\mathbf{B}^e \equiv \begin{bmatrix}
[L_{i,x}] & \mathbf{0} & \mathbf{0} & \mathbf{0} & \mathbf{0} & \mathbf{0} & \mathbf{0} \\
\mathbf{0} & [L_{i,y}] & \mathbf{0} & \mathbf{0} & \mathbf{0} & \mathbf{0} & \mathbf{0} \\
[L_{i,y}] & [L_{i,x}] & \mathbf{0} & \mathbf{0} & \mathbf{0} & \mathbf{0} & \mathbf{0} \\
\mathbf{0} & \mathbf{0} & \mathbf{0} & [L_{i,x}] & \mathbf{0} & \mathbf{0} & \mathbf{0} \\
\mathbf{0} & \mathbf{0} & \mathbf{0} & \mathbf{0} & \mathbf{0} & [L_{i,x}] & \mathbf{0} \\
\mathbf{0} & \mathbf{0} & \mathbf{0} & \mathbf{0} & [L_{i,y}] & \mathbf{0} & \mathbf{0} \\
\mathbf{0} & \mathbf{0} & \mathbf{0} & \mathbf{0} & \mathbf{0} & \mathbf{0} & [L_{i,y}] \\
\mathbf{0} & \mathbf{0} & \mathbf{0} & [L_{i,y}] & [L_{i,x}] & \mathbf{0} & \mathbf{0} \\
\mathbf{0} & \mathbf{0} & \mathbf{0} & \mathbf{0} & \mathbf{0} & [L_{i,y}] & \mathbf{0} \\
\mathbf{0} & \mathbf{0} & \mathbf{0} & \mathbf{0} & \mathbf{0} & \mathbf{0} & [L_{i,x}] \\
\mathbf{0} & \mathbf{0} & [L_{i,y}] & \alpha[L_{1i,y}] & \alpha[L_{2i,y}]+[L_i] & \alpha c[L_{1i,y}] & \alpha c[L_{2i,y}] \\
\mathbf{0} & \mathbf{0} & \mathbf{0} & \mathbf{0} & \mathbf{0} & \mathbf{0} & [L_i] \\
\mathbf{0} & \mathbf{0} & [L_{i,x}] & \alpha[L_{1i,x}]+[L_i] & \alpha[L_{2i,x}] & \alpha c[L_{1i,x}] & \alpha c[L_{2i,x}] \\
\mathbf{0} & \mathbf{0} & \mathbf{0} & \mathbf{0} & \mathbf{0} & [L_i] & \mathbf{0}
\end{bmatrix} \quad \text{(A2)}$$

where $i=1,2,3$, $k=1,m_{12},2,m_{23},3,m_{31}$, and where $\mathbf{0}$ is a null row vector.

REFERENCES

[1] D. Liu and X. Li. An overall view of laminate theories based on displacement hypothesis. Journal of Composite Materials, 30(14):1539–1561, 1996.

[2] E. Reissner. On a certain mixed variational theorem and a proposed application. International Journal for Numerical Methods in Engineering, 20(7):1366–1368, 1984.

[3] J.N. Reddy. Mechanics of laminated composite plates. CRC Press, NewYork, 1997.

[4] E. Reissner and Y. Stavsky. Bending and stretching of certain types of heterogeneous aeolotropic elastic plates. Journal of Applied Mechanics, 28(3):402–408, 1961.

[5]   R.D. Mindlin. Influence of rotatory inertia and shear deformation on flexural motions of isotropic elastic plates. Journal of Applied Mechanics,(18):31–38, 1951.

[6]   J.M. Whitney and N.J. Pagano. Shear deformation in heterogeneous anisotropic plates. Journal of Applied Mechanics, 37(4):1031–1036, 1970.

[7]   E. Reissner. Reflections on the theory of elastic plates. Applied Mechanics Reviews, 38(11):1453–1464, 1985.

[8]   L. Librescu, A. Khdeir, and J. Reddy. A comprehensive analysis of the state of stress of elastic anisotropic flat plates using refined theories. Acta Mechanica, 70:57–81, 1987.

[9]   A.K. Noor and W.S. Burton. Assessment of shear deformation theories for multilayered composite plates. Applied Mechanics Reviews, 42(1):1–13, 1989.

[10] J.N. Reddy. A simple higher-order theory for laminated composite plates. Journal of Applied Mechanics, 51(4):745–752, 1984.

[11] A. Tessler. An improved plate theory of {1,2}-order for thick composite laminates. International Journal of Solids and Structures, 30(7):981 – 1000, 1993.

[12] G.M. Cook and A. Tessler. A {3,2}-order bending theory for laminated composite and sandwich beams. Composites Part B: Engineering, 29(5):565 – 576, 1998.

[13] A. Barut, E. Madenci, T. Anderson, and A. Tessler. Equivalent single-layer theory for a complete stress field in sandwich panels under arbitrarily distributed loading. Composite Structures, 58(4):483 – 495, 2002.

[14] J.N. Reddy. A generalization of two-dimensional theories of laminated composite plates. Communications in Applied Numerical Methods,3(3):173–180, 1987.

[15] X. Lu and D. Liu. An interlaminar shear stress continuity theory for both thin and thick composite laminates. Journal of Applied Mechanics, 59(3):502–509, 1992.

[16] A. Toledano and H. Murakami. A high-order laminated plate theory with improved in-plane responses. International Journal of Solids and Structures, 23(1):111–131, 1987.

[17] A. Toledano and H. Murakami. A composite plate theory for arbitrary laminate configurations. Journal of Applied Mechanics, 54(1):181–189, 1987.

[18] M. Di Sciuva. A refinement of the transverse shear deformation theory for multilayered orthotropic plates. In Proceedings of 7th AIDAA National Congress, 1983; also in L'aerotecnica missili e spazio, 62, 84-92, 1984.

[19] M. Di Sciuva. A refined transverse shear deformation theory for multilayered anisotropic plates. Atti Accademia delle Scienze di Torino, (118):279–295, 1984.

[20] M. Di Sciuva. Development of an anisotropic, multilayered, shear-deformable rectangular plate element. Computers & Structures, 21(4):789 – 796, 1985.

[21] M. Di Sciuva. Evaluation of some multilayered, shear-deformable plate elements. In Proceedings of 26th Structures, Structural Dynamics and Materials Conference, pages 394 – 400. AIAA/ASME/ASCE/AHS-Paper 85-0717, 1985.

[22] M. Di Sciuva. Bending, vibration and buckling of simply supported thick multilayered orthotropic plates: An evaluation of a new displacement model. Journal of Sound and Vibration, 105(3):425 – 442, 1986.

[23] H. Murakami. Laminated composite plate theory with improved in-plane responses. Journal of Applied Mechanics, 53(3):661–666, 1986.

[24] M. Di Sciuva. An improved shear-deformation theory for moderately thick multilayered anisotropic shells and plates. Journal of Applied Mechanics, 54(3):589–596, 1987.

[25] R.C. Averill. Static and dynamic response of moderately thick laminated beams with damage. Composites Engineering, 4(4):381 – 395, 1994.

[26] M. Di Sciuva. Further refinement in the transverse shear deformation theory for multilayered composite plates. Atti Accademia delle Scienze di Torino, (124(5-6)):248–268, 1990.

[27] M. Di Sciuva. Multilayered anisotropic plate models with continuous interlaminar stresses. Composite Structures, 22(3):149 – 167, 1992.

[28] M. Cho and R.R. Parmenter. Efficient higher order composite plate theory for general lamination configurations. AIAA Journal, 31(7):1299–1306, 1993.

[29] M. Di Sciuva, M. Gherlone, and L. Librescu. Implications of damaged interfaces and of other non-classical effects on the load carrying capacity of multilayered composite shallow shells. International Journal of NonLinear Mechanics, 37(4-5):851 – 867, 2002.

[30] R.C. Averill and Y.C. Yip. Development of simple, robust finite elements based on refined theories for thick laminated beams. Computers and Structures, 59(3):529–546, 1996.

[31] P. Umasree and K. Bhaskar. Analytical solutions for flexure of clamped rectangular cross-ply plates using an accurate zig-zag type higher-order theory. Composite Structures, 74(4):426 – 439, 2006.

[32] A. Tessler, Di Sciuva, and M. Gherlone. A refined linear zigzag theory for composite beams: reformulation of zigzag function and shear stress constraints, VI International Symposium on Advanced Composites and Applications for the New Millennium, Corfù, Greece, May 2007.

[33] A. Tessler, M. Di Sciuva, and M. Gherlone. Refinement of Timoshenko beam theory for composite and sandwich beams using zigzag kinematics. Technical Report NASA/TP-2007-215086, NASA, December 2007.

[34] A. Tessler, M. Di Sciuva, and M. Gherlone. A refined zigzag beam theory for composite and sandwich beams. Journal of Composite Materials, 43(9):1051–1081, 2009.

[35] A. Tessler, M. Di Sciuva, and M. Gherlone. A Shear-Deformation Theory for Composite and Sandwich Plates using Improved Zigzag Kinematics. Proceedings of 9th International Conference on Computational Structures Technology, Athens, Greece, September 2008.

[36] A. Tessler, M. Di Sciuva, and M. Gherlone. Refined zigzag theory for laminated composite and sandwich plates. Technical Report NASA/TP-2009-215561, NASA, January 2009.

[37] A. Tessler, M. Di Sciuva, and M. Gherlone. A consistent refinement of first-order shear-deformation theory for laminated composite and sandwich plates using improved zigzag kinematics. Journal of Mechanics of Materials and Structures, 5(2):341–367, 2010.

[38] A. Tessler, M. Di Sciuva, and M. Gherlone. Refined zigzag theory for homogeneous, laminated composite, and sandwich plates: a homogeneous-limit methodology for zigzag function selection. Technical Report NASA/TP-2010-216214, NASA, January 2010.

[39] A. Tessler, M. Di Sciuva, and M. Gherlone. A homogeneous limit methodology and refinements of computationally efficient zigzag theory for homogeneous,

laminated composite, and sandwich plates. Numerical Methods for Partial Differential Equations, 27(1):208–229, 2011.

[40] T.J.R. Hughes, R.L. Taylor, and W. Kanoknukulchai. A simple and efficient finite element for plate bending. International Journal for Numerical Methods in Engineering, 11(10):1529–1543, 1977.

[41] T.J.R. Hughes. The C^0-Approach to Plates and Beams. Prentice-Hall, 1987.

[42] O.C. Zienkiewicz and R.L. Taylor. The finite element method for solid and structural mechanics. Elsevier, 6th edition, 2005.

[43] A. Tessler and S.B. Dong. On a hierarchy of conforming Timoshenko beam elements. Computers & Structures, 14(3-4):335 – 344, 1981.

[44] A. Tessler. An efficient, conforming axisymmetric shell element including transverse shear and rotary inertia. Computers & Structures, 15(5):567– 574, 1982.

[45] A. Tessler and T.J.R. Hughes. A three-node Mindlin plate element with improved transverse shear. Computer Methods in Applied Mechanics and Engineering, 50(1):71 – 101, 1985.

[46] A. Tessler. A priori identification of shear locking and stiffening in triangular Mindlin elements. Computer Methods in Applied Mechanics and Engineering, 53(2):183 – 200, 1985.

[47] A. Tessler. Shear-deformable, anisoparametric flexure elements with penalty relaxation (Chapter 11). Finite element methods in plate and shell structures (Book, eds. T.J.R. Hughes and E. Hinton), Pineridge Press, London, 1986.

[48] I. Fried, A.R. Johnson, and A. Tessler. Minimum-degree thin triangular plate and shell bending finite elements of order two and four. Computer Methods in Applied Mechanics and Engineering, 56:283–307, 1986.

[49] A. Tessler and L. Spiridigliozzi. Curved beam elements with penalty relaxation. International Journal for Numerical Methods in Engineering, 23(12):2245–2262, 1986.

[50] A. Tessler and L. Spiridigliozzi. Resolving membrane and shear locking phenomena in curved shear-deformable axisymmetric shell elements. International Journal for Numerical Methods in Engineering, 26(5):1071–1086, 1988.

[51] A. Tessler. A C^0-anisoparametric three-node shallow shell element. Computer Methods in Applied Mechanics and Engineering, 78(1):89 – 103, 1990.

[52] A. Barut, E. Madenci, and A. Tessler. Nonlinear elastic deformations of moderately thick laminated shells subjected to large and rapid rigid-body motion. Finite Elements in Analysis and Design, 22(1):41 − 57, 1996.

[53] A. Barut, E. Madenci, and A. Tessler. Nonlinear analysis of laminates through a Mindlin-type shear deformable shallow shell element. Computer Methods in Applied Mechanics and Engineering, 143(1-2):155 −173, 1997.

[54] A. Barut, E. Madenci, A. Tessler, and J.H. Starnes Jr. A new stiffened shell element for geometrically nonlinear analysis of composite laminates. Computers & Structures, 77(1):11 − 40, 2000.

[55] J. Liu, H.R. Riggs, and A. Tessler. A four-node, shear-deformable shell element developed via explicit Kirchhoff constraints. International Journal for Numerical Methods in Engineering, 49(8):1065–1086, 2000.

[56] A. Barut, E. Madenci, and A. Tessler. Nonlinear thermoelastic analysis of composite panels under non-uniform temperature distribution. International Journal of Solids and Structures, 37(27):3681 − 3713, 2000.

[57] A. Tessler. Comparison of Interdependent Interpolations for Membrane and Bending Kinematics in Shear-Deformable Shell Elements. Proceedings of Intern. Conf. on Computational Engineering Science (ICES2K), Los Angeles, CA. August 2000.

[58] A. Tessler and J. W. Mohr. A three-node shell element with drilling degrees of freedom for thick composite and sandwich structures. Proceedings of IASS-IACM 2000 Colloquium on Computation of Shell and Spatial Structures, Athens, Greece, June 2000.

[59] M. Gherlone, A. Tessler, and M. Di Sciuva. A C^0-continuous two-node beam element based on refined zigzag theory and interdependent interpolation. MAFELAP 2009 Conference, Brunel University, London (UK), June 2009.

[60] M. Gherlone, A. Tessler, and M. Di Sciuva. C^0 beam elements based on the refined zigzag theory for multilayered composite and sandwich laminates. Composite Structures, 93(11):2882 − 2894, 2011.

[61] D. Versino, M. Mattone, M. Gherlone, A. Tessler, and M. Di Sciuva. An efficient, C^0-continuous triangular element for laminated composite and sandwich plates with improved zigzag kinematics. MAFELAP 2009 Conference, Brunel University, London (UK), June 2009.

[62]   E. Reissner. The effect of transverse shear deformation on the bending of elastic plates. Journal of Applied Mechanics, 12:68–77, 1945.

[63]   D.T. Guzzafame. Finite element formulation for the analysis of multilayered plates in cylindrical bending. M.S. Thesis, Politecnico di Torino, October 2006.

[64]   C. Fasano C. Development and implementation of interface techniques for beam finite elements. M.S. Thesis (in Italian), Politecnico di Torino, March 2008.

[65]   N.J. Pagano. Exact solutions for rectangular bidirectional composites and sandwich plates. Journal of Composite Materials, 1(4):20–34, 1970.